PHYSICAL REVIEW C VOLUME 36, NUMBER 2 AUGUST 1987

Off-energy-shell behavior of realistic potential models

Edward F. Redish*
Department of Physics and Cyclotron Facility, Indiana University, Bloomington, Indiana 47405

Karen Stricker-Bauer
Lockheed Palo Alto Research Laboratory, Palo Alto, California 94304
(Received 10 November 1986)

The behavior of the fully-off-the-energy-shell T matrices for the Reid-soft-core and Paris-80 potentials are studied for a variety of partial waves, both uncoupled and coupled. Although the potentials have qualitatively different structures in both coordinate space and momentum space, the resulting off-energy-shell behavior is very similar in the range of energy and momentum relevant to low and medium energy nuclear physics.

I. INTRODUCTION

Because of the strength of the two-nucleon force, the off-energy-shell T matrix or four-point function is a natural and convenient way of putting two-particle information into many-particle calculations. This is particularly the case in those areas of nuclear physics which come closest to having a complete and convergent calculational scheme based on two-body forces, such as the three-body problem,[1] multiple-scattering theory of intermediate energy elastic and inelastic nucleon-nucleus scattering,[2] and the theory of nuclear matter.[3]

The off-shell T matrix also provides a convenient interface between the physical assumptions made in traditional nuclear physics about the two-nucleon system and the resulting implications for many-particle calculations. It has been known for many years that reactions which directly depend on the half-shell T matrix, such as bremsstrahlung[4] or knockout,[5] require the use of the half-shell amplitude rather than an on-shell one, and that, further, the half-shell amplitudes from realistic potential models are rather well determined[6] given the on-shell amplitude, the long and intermediate range part of the potential, and the assumptions that the relative wave function is smooth and suppressed in the interior.

The fully-off-shell nucleon-nucleon T matrix has, unfortunately, not previously received the kind of systematic and detailed study which is required to understand the relation of the two-nucleon input information both to the many-particle results and to the underlying physical assumptions. This paper is part of a broad study in which we consider the behavior of the off-shell T matrices produced by nonrelativistic potential models and the implications of the resulting systematics for many-body calculations. As a first step, we consider here the fully-off-shell behavior of the T matrices from two potentials which are realistic but which have a severely different character: the Reid soft core (RSC) potential[7] and the Paris-80 (P80) potential.[8]

The RSC potential is the widely used standard of the previous decade. It has a one pion exchange potential (OPEP) tail, a midrange attraction, and short-range repulsion. The ranges are chosen from consideration of the possible mesons that can be exchanged, and the strengths (except for OPEP) are adjusted to fit the two-body data.

The P80 potential has become the standard of the 1980s. In addition to the OPEP, its midrange potential is constructed from the meson theory of the exchange of two interacting pions using dispersion relations and a reasonable (if arbitrary) ansatz for an off-shell continuation. At short range the potential is parametrized following a complicated procedure. This will be discussed in more detail below.

Both potentials lead to excellent fits of the data, with P80 being somewhat superior (see Fig. 1). The RSC potential is given in each partial wave, while P80 is given in the form of a central, spin-orbit, tensor, plus quadratic spin-orbital potential. It contains a strong explicit nonlocality of very short range in the form of a velocity dependence. When considered either in coordinate or momentum space, it is clear that the short-range physical content of these two potentials is very different.

We note that recently the Bonn group[9] has made substantial advances in the calculation of meson theoretic potentials and there are indications of both improvements in the fit to on-shell data[10] and in the fit to the triton binding energy.[11] An analysis of the Born potential is planned for a subsequent work.

In this paper we compare the off-shell behavior of RSC and P80 in partial waves for $J \leq 2$. In Sec. II we introduce notation. In Sec. III we discuss the character of the potentials and their structure in momentum space. Our method of solving the Lippmann-Schwinger (LS) equation is presented in Sec. IV. Included there is a discussion of the convergence of our quadrature rule. In Sec. V we present our results for the off-shell amplitudes. An analysis of our results is presented in Sec. VI; conclusions follow in Sec. VII.

II. THE OFF-SHELL T MATRIX

The full T matrix contains all the information about the two-body bound and scattering states in a more direct way than the potential does. For a system of particles interacting by strong, short-range forces, the interactions of any pair must be summed to all orders in any arrange-

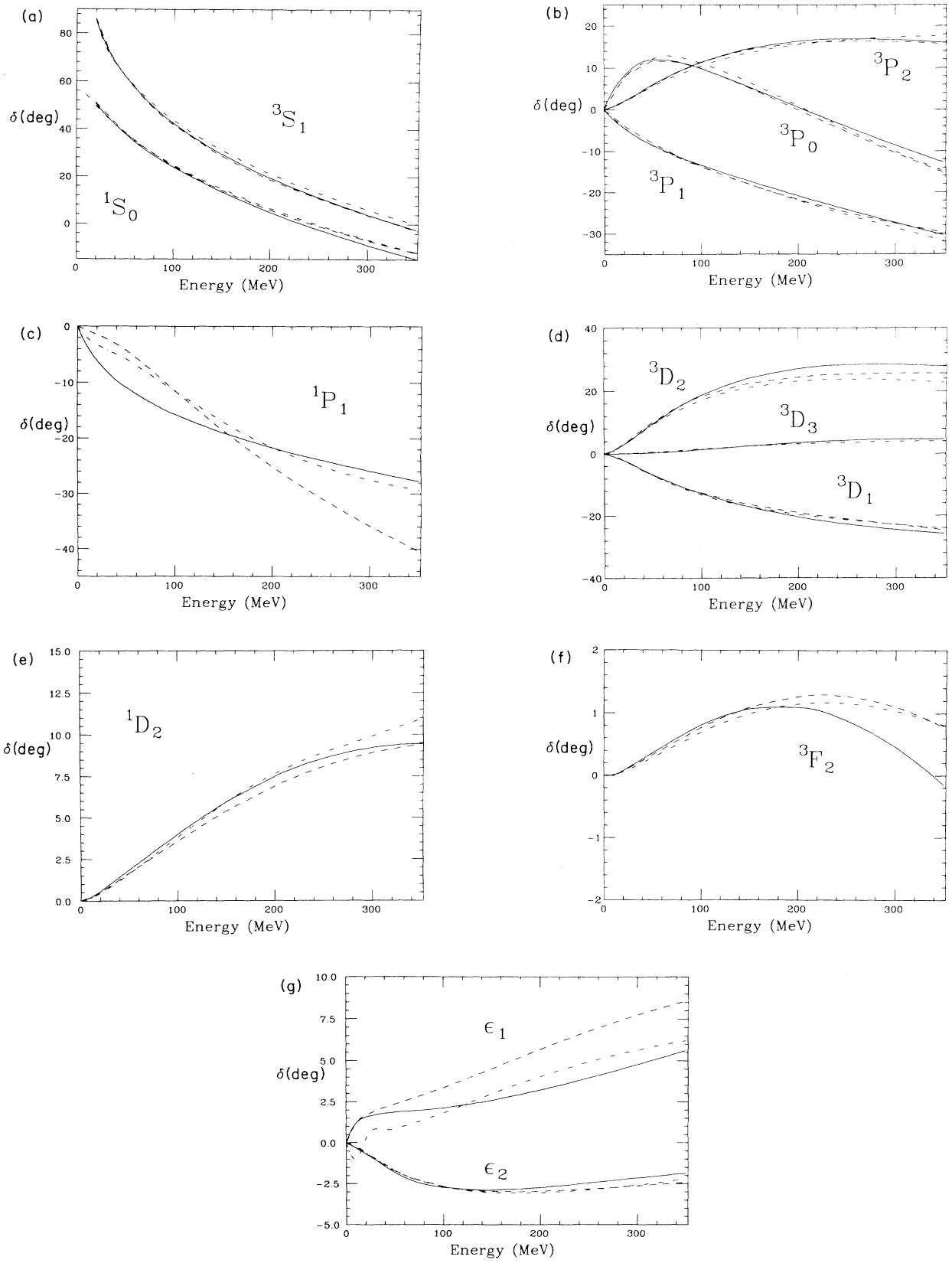

FIG. 1. Nuclear bar phase shifts given by P80 potential (solid), RSC potential (dashed), and the VPI-SP86 phase shift analysis (dotted-dashed) as a function of lab energy.

ment of the many-body theory. For a number of important cases this makes off-shell amplitudes a convenient starting point.

We work with the off-shell two-body T matrix defined by the operator relation

$$T(z)=V+VG(z)V\ , \tag{1}$$

where V is the two-body potential and $G(z)$ is the full Green's function

$$G(z)=1/(z-H)\ . \tag{2}$$

H is the full Hamiltonian, $H=H_0+V$, where H_0 is the operator for the kinetic energy of relative motion of the two particles. The matrix elements of $T(z)$ have a cut along the real axis. The value of the matrix element is to be taken as the cut is approached from above in the complex plane. This is indicated by the notation $z=e+i\epsilon\equiv E^+$ and provides the outgoing-wave boundary conditions needed to make the proper identifications with scattering theory.[12] The two-body bound state information is present since $T(z)$ has a pole at the energy $z=-\epsilon_b$, where ϵ_b is the binding energy.

The resolvent relation for $G(z)$ is

$$G(z)=G_0(z)+G_0(z)VG(z)\ , \tag{3}$$

where $G_0(z)$ is the free Green's function $1/(z-H_0)$. It may be used to obtain the operator Lippman-Schwinger equation[13] for T,

$$T(z)=V+VG_0(z)T(z)\ . \tag{4}$$

We work in the center of mass frame for the two particles. For equal mass particles, the energies quoted will therefore be half the lab energy. The two-body scattering amplitude is given by the on-shell matrix element of T,

$$f(E_k,\theta)=-(\mu/2\pi\hbar^2)\langle \mathbf{k}' \mid T(E_k) \mid \mathbf{k}\rangle\ , \tag{5}$$

where θ is the angle between $\mathbf{k}$ and $\mathbf{k}'$ and $E_k^+=k^2/2\mu=k'^2/2\mu$ with μ equal to the reduced mass. The half-shell matrix elements of T have the form $\langle \mathbf{k}' \mid T(E_k) \mid \mathbf{k}\rangle$ with $k'^2/2\mu$ not equal to $E_k=k^2/2\mu$. The fully-off-shell T matrix elements are $\langle \mathbf{k}' \mid T(E^+) \mid \mathbf{k}\rangle$ with $k^2/2\mu\neq E$.

We will use the partial-wave decomposition of the matrix elements of Eq. (4) in momentum space to solve for T explicitly. For the uncoupled states (or in the absence of tensor forces) the partial-wave expansion is

$$\langle \mathbf{k}' \mid T(z) \mid \mathbf{k}\rangle=(4\pi)^2\sum Y_{lm}(\Omega')^*t_l(k',k;2\mu z)Y_{lm}(\Omega)\ , \tag{6a}$$

$$\langle \mathbf{k}' \mid V \mid \mathbf{k}\rangle=(4\pi)^2\sum Y_{lm}(\Omega')^*v_l(k',k)Y_{lm}(\Omega)\ . \tag{6b}$$

We have assumed that the potential is energy independent, but it may be nonlocal. The Lippman-Schwinger equation (4) in partial-wave form is

$$t_l(k,k';p^2)=v_l(k,k')+(2/\pi)\int_0^\infty dq\,q^2v_l(k,q)\times 2\mu(p^2-q^2+i\epsilon)^{-1}\times t_l(q,k';p^2)\ . \tag{7}$$

This equation is almost in a form appropriate for calculation. However, since the Green function is complex by the equation

$$\lim_{-\epsilon\to 0}(x+i\epsilon)^{-1}=(x)_p^{-1}-i\pi\,\delta(x)\ , \tag{8}$$

where $(\cdots)_p$ indicates the principal value, the function t_l will be complex. We reduce the storage requirements for the calculation by handling the complex part of the pole explicitly, solving a real integral equation, and subsequently performing algebraic manipulations to yield the complex T matrix. This is done by solving the K-matrix equation

$$k_l(k,k';p^2)=v_l(k,k')+(2/\pi)\int_0^\infty dq\,q^2v_l(k,q)\times 2\mu(p^2-q^2)_P^{-1}\times k_l(q,k';p^2)\ . \tag{9}$$

The partial-wave K matrix, $k_l(k,k';p^2)$ is then related to the partial-wave T matrix by the Heitler equation,[12]

$$t_l(k,k';p^2)=k_l(k,k';p^2)-\frac{2i\mu p k_l(k,p;p^2)k_l(p,k';p^2)}{1+2i\mu p k_l(p,p;p^2)}\ . \tag{10}$$

When tensor forces are present, the partial-wave expansion includes different angular momenta for the initial and final states. For the tensor coupled states, Eqs. (6) become

$$\langle \mathbf{k}' \mid T(z) \mid \mathbf{k}\rangle=(4\pi)^2\sum Y_{l'm}(\Omega')^*t_{l'l}(k',k;2\mu z)Y_{lm}(\Omega)\ , \tag{11a}$$

$$\langle \mathbf{k}' \mid V \mid \mathbf{k}\rangle=(4\pi)^2\sum Y_{l'm}(\Omega')^*v_{l'l}(k'k)Y_{lm}(\Omega)\ . \tag{11b}$$

The equation for the coupled states is

$$k_{l'l}(k',k;p^2)=v_l(k',k)+(2/\pi)\sum_{l''}\int_0^\infty dq\,q^2v_{l'l''}(k',q)\times 2\mu(p^2-q^2)_P^{-1}\times k_{l''l}(q,k;p^2)\ , \tag{12}$$

while the Heitler equation is

$$t_{l'l}(k',k;p^2)=k_{l'l}(k',k;p^2)-2i\mu p\sum k_{l'l''}(k',p;p^2)[\mathbf{1}+2i\mu p\,\mathbf{k}(p,p;p^2)]^{-1}_{l''l'''}k_{l'''l'}(p,k;p^2)\ . \tag{13}$$

We have written $\mathbf{1}$ for the matrix $\delta_{l'l}$ and $\mathbf{k}$ for the matrix $k_{l'l}$.

For the nucleon-nucleon system, both particles have spin $\frac{1}{2}$ and the interactions conserve total angular momentum and parity. As a result, in a state having total angular momentum j, the tensor forces can only couple states

of orbital angular momentum $l=j+1$ and $j-1$. The sums in Eqs. (12) and (13) therefore never have more than two terms.

The relation of the on-shell T and K matrices to the phase shifts in the uncoupled states is given by

$$t_l^{\rm on}(p)\equiv t_l(p,p;p^2)=-(\hbar^2/2\mu)e^{i\delta_l(p)}\sin\delta_l(p)/p \ , \quad (14)$$

$$k_l^{\rm on}(p)\equiv k_l(p,p;p^2)=-(\hbar^2/2\mu)\tan\delta_l(p)/p \ . \quad (15)$$

For the coupled states, there are two conventions in common use: the Blatt-Biedenharn[14] and Stapp-Ypsilantis-Metropolis[15] conventions. We will present our results using the latter (nuclear bar phase shifts). In this convention, the on-shell K matrices are related to the phase shift δ_+ and δ_- (corresponding to orbital angular momenta $j+1$ and $j-1$, respectively) and mixing parameter ϵ. If we define

$$\mathbf{K}=\begin{bmatrix} k_- & k \\ k & k_+ \end{bmatrix} , \quad (16)$$

$$\begin{aligned} &\Sigma=(2\mu p/\hbar c)(k_- - k_+) \ , \\ &\Delta=(2\mu p/\hbar c)(k_- k_+) \ , \\ &\mathcal{L}=(2\mu p/\hbar c)^2(k_- k_+ - k^2) \ , \end{aligned} \quad (17)$$

$$\begin{aligned} &\tan 2\sigma=\Sigma/(1-\mathcal{L}) \ , \\ &\tan 2\tau=\Delta/(1+\mathcal{L}) \ , \end{aligned} \quad (18)$$

then the phase shifts and mixing parameter are given by

$$\begin{aligned} &\delta_-=\sigma+\tau \ , \\ &\delta_+=\sigma-\tau \ , \\ &\tan 2\epsilon=2k/[(1+\mathcal{L})^2+\Delta^2]^{1/2} \ . \end{aligned} \quad (19)$$

III. THE RSC AND P80 POTENTIALS

In this section we describe the structure of the Reid soft core and the Paris-80 potentials paying particular attention to their momentum space matrix elements.

A. The RSC potential

Reid's soft-core potential[7] is given explicitly in coordinate space for the partial waves of total angular momentum less than or equal to 2. It is specified individually in each partial wave as a local radial potential written as the sum of Yukawas and Yukawas times powers of $1/r$. The fact that the radial potential differs in different partial waves implies that when the momentum space matrix elements of the potential are built up by Eq. (6b), the potential will be L dependent (i.e., have some angular nonlocality). This will not be easily represented by the standard angular nonlocalities such as spin-orbit, quadratic spin-orbit, or simple L dependent forces, since the ranges and number of terms vary from one partial wave to the next.

The strengths and ranges of the potential terms are set up in the spirit of the one-boson-exchange (OBE) model. The longest range term is taken to be that arising from one-pion exchange (OPE) with the appropriate strength and range. Shorter ranged terms are taken to correspond approximately to a midrange attraction coming from the exchange of a fictitious sigma meson (with a mass of 4 pion masses) and a short range repulsion arising from the exchange of an omega (with a mass of 7 pion masses). Ranges of 2, 3, and 6 pion masses are also used in some channels. The strengths of the non-OPE terms were adjusted to fit the two-body bound-state and phase-shift information available at the time.

The matrix elements of the RSC potential in momentum space require the partial wave Fourier transform of the potentials:

$$A(x)=\exp(-x)/x \ , \quad (20a)$$

$$B(x)=(1+3/x+3/x^2)\exp(-x)/x \quad (20b)$$

for $x=\mu r$, where μ is the inverse range (meson mass). These are given by

$$O_{ll'}(k,k',\mu)=\int r^2 dr\, j_l(kr)O(\mu r)j_{l'}(k'r) \quad (21)$$

for $O=A$ and B. The particular matrix elements required are $O_{ll}=O_l$ and $O_{j-1\,j+1}=O^j$ (for the coupled states). For A_l, B_l, and B^j the closed form results are[16]

$$A_l(k,k',\mu)=Q_l(y)/2kk'\mu \ , \quad (22)$$

$$B_l(k,k',\mu)=A_l(k,k'\mu) +3[Q_{l-1}(y)-Q_{l+1}(y)]/2\mu^3(2l+1) \ , \quad (23)$$

$$B^j(k,k')=[k'Q_{j-1}(y)/2k+kQ_{j+1}/2k'-Q_j(y)]/\mu^3 \ , \quad (24)$$

where Q_i is the ith Legendre function of the second kind[17] and y is the combination

$$y=(k^2+k'^2+\mu^2)/2kk' \ . \quad (25)$$

The off-diagonal matrix element A^j is obtained recursively. Using the recursion relation for the spherical Bessel functions,[17] we obtain the result

$$A^j=\{[(2j+1)/(2j-1)](k'/k)Q_j(y)-Q_{j-1}(y)\}/2\mu k'^2 +[(2j+1)/(2j-1)](k/k')A^{j-1} \ . \quad (26)$$

For $j=0$ the integral can be performed explicitly and yields

$$A^j=(6kk'+(3^2+k'^2-3k^2)Q_0(y) +6k\{\tan^{-1}[\mu/(k'-k)] -\tan^{-1}[\mu/(k'+k)]\})/4kk'^3\mu \ . \quad (27)$$

It is well known that recursing Bessel functions upwards is inherently unstable. Nonetheless, we find that for $z\equiv k'/\mu<0.5$ the upward recursion is accurate when the index j is less than 6. For larger values of k' we begin at a large value of j and recurse downward. For large j, the Bessel functions in (21) may be approximated by their small argument form and the integrals done analytically. The result is

$$A^j\simeq(C_j/\mu^3)(kk'/\mu^2)^j(k'/k) \ , \quad (28)$$

where

$$C_j = 4^j(2j+1)j!(j+2)!/(2j+4)! \ . \tag{29}$$

The downward recursion is stable and the results are independent of the starting value of j once it is above a critical value. This value is dependent on z, since if z is too large one must go to a larger value of the index j before the small argument expansion of the Bessel function can be used.

If the starting j gets too large, very many terms must be calculated and the code slows down significantly. Since the upward and downward recursions have complementary regions of validity, we use upward recursion for $z < 0.5$ and downward for $z > 0.5$. We begin our downward recursion at $j = 10$ for z less than 0.1 and at 20 otherwise. This procedure provides six-figure accuracy throughout.

For partial waves with $j > 2$ Reid recommends using OPEP, although for energies near the upper end of the potential scattering region ($E \sim 350$ MeV) this may not be adequate. An extended version of the Reid potential describing partial waves with j greater than 2 has been created by Day.[18] We do not consider these states here.

The natural scale of the RSC potential in momentum space is determined by the shortest range (largest mass) used in the parametrization. Since this is 4.9 fm^{-1} (7 pion masses), we expect that most of the action in solving the integral equation (15) in momentum space will occur inside about 8–10 fm^{-1}.

B. The Paris-80 potential

The potential known as Paris-80 (P80) was obtained as a result of many years of effort.[19,8] The primary improvement over earlier potentials is the combination of a detailed treatment of the intermediate range attraction, together with a high quality phenomenological adjustment to the two-body data.

In the model of the nucleon-nucleon force arising from the suppression of mesonic degrees of freedom, the potential arises from the exchange of one or more mesons. One possible way of handling multiple meson exchange is by observing that much of the low energy meson spectrum is dominated by resonances. If these are treated as single mesons with well defined masses, potentials arising from their exchange can be calculated. Such a model is referred to as one-boson-exchange potential (OBEP).[9]

Unfortunately, the midrange part of the force does not seem to be well approximated in this way. The S-wave interaction of two pions shows a broad maximum in the neighborhood of about 500 MeV, but it is not sharp enough to be called a resonance. In addition, one expects significant contributions to the midrange potential from the exchange of two pions in which one of the nucleons becomes a delta between the exchanges. This is also not easily representable as the exchange of a single boson.

The Paris group uses dispersion relations to extrapolate the on-shell π-nucleon scattering amplitude to unphysical values of the momentum. This sums the result of all two-pion exchanges including uncrossed and crossed pion lines, strongly interacting pions and exchanges in which one of the intermediate nucleons is in an excited state. In order to use this result in a potential, it must be continued off shell. An arbitrary ansatz is chosen to provide the off-shell continuation. (The off-shell amplitude is assumed local.) This yields an effective two-pion exchange potential (TPEP). The three-meson exchange terms are approximated by an ω meson, generally assumed (in OBEP models) to be responsible for the strong short-range repulsion.

The three terms together (OPEP, TPEP, and ω exchange) yield an intermediate range potential which is in good qualitative agreement with older, more phenomenological potentials for $r > 1.4$ fm.

In order to obtain a complete potential, the midrange part was taken to go over smoothly to a flat core in the interior. The height of the core was adjusted to fit the empirical phase shifts at each energy. The central and spin-orbit potentials were found to vary linearly with energy.

For the Paris-80 parametrization the linear energy dependence has been transformed into a momentum dependence. This may be done as follows. Assume that ψ satisfies the Schrödinger equation with a linear energy-dependent potential

$$[p^2/2\mu + U(r) + EW(r)]\psi(r) = E\psi(r) \ . \tag{30}$$

A new wave function may be defined,

$$\phi(r) = (1-W)^{1/2}\psi(r) \ , \tag{31}$$

which satisfies a related equation

$$[(1-W)^{-1/2}(p^2/2\mu)(1-W)^{-1/2} + U/(1-W)]\phi(r) = E\phi(r) \ . \tag{32}$$

If we expand $(1-W)^{-1/2}$ in powers of W and only keep the first term, we will see that ϕ satisfies an approximate Schrödinger equation with the effective potential

$$V_{\text{eff}}(r,p) = U/(1-W) + \tfrac{1}{2}(p^2W + Wp^2) \ . \tag{33}$$

The p's in this equation are to be considered operators.

One should note two things about this procedure. First, in making the transformation (31), we are not changing the phase shifts. The function W vanishes at large distances to ϕ and ψ, which are identical asymptotically. However, if we interpret ϕ to be the Schrödinger wave function rather than ψ, then the off-shell T matrix will be changed since it depends on the wave function inside the range of the potential. Second, this phase equivalence only holds for Eqs. (30) and (32). The approximate potential (33) does not give the same phase shifts as Eq. (32).

As a final step, the Paris group provides a convenient form for use in nuclear calculations by fitting the coordinate space forms with the sum of (a rather large number of) Yukawas. Since a potential of the form (33) is used, the parameters of the Yukawian form had to be adjusted to produce a better fit to the two-nucleon data.[8] Twelve terms are used with ranges corresponding to exchanged meson masses varying between 135 MeV (range of 1.46 fm, the OPEP) and 2.226 GeV (a range of 0.09 fm).

The use of the p^2 terms in the potential produces some unusual effects. First, the introduction of an explicit nonlocality into the potential reduces the coupling

between various elements of the two-body input and permits somewhat more flexibility than is obtained with local potentials.[20] For example, the percentage deuteron D state is an off-shell parameter since it measures a property of the wave function inside the range of the potential. (In contrast, the asymptotic D/S ratio may be thought of as an on-shell property.) In a local model, this is strongly constrained by the experimental value of the deuteron's quadrupole moment, and usually comes out to be about 7% (RSC=6.5%, Reid hard core=6.5%, Hamada-Johnson=7.0%, Bressel-Kerman-Rouben=6.5%).[21] In a nonlocal model such as Paris-80, this can be reduced and turns out to be 5.8%.[8] (In some of the new Bonn potentials[9] it is as low as 4.3%.)

Second, it has been known for many years[22] that nuclear matter is infinitely bound when p^2-type potentials are present which have coefficient functions that have some negative part in coordinate space. The collapse occurs because sharply oscillatory two body correlations at the right distance lead to an arbitrarily strong attraction. The p^2 pair potentials contribute an attraction proportional to N^2 and dominate the kinetic energy operator which contributes a repulsion proportional to N for large numbers of particles. This problem is avoided in practice by working with variational wave functions which do not have the types of two-body correlations that would lead to collapse. It has yet to be demonstrated that this is a sensible resolution of the problem.

Third, the use of p^2 terms in the potential drives the natural momentum scale up to very high values—even higher than the 11.3 fm^{-1} associated with the Yukawa of shortest range that is present in the Paris-80 expansion. To see why this occurs, let us consider the asymptotic form of the nonlocal, central part of the P80 potential. In momentum space this is

$$\langle \mathbf{k}' \mid V_C^{\rm nl} \mid \mathbf{k} \rangle = (k^2+k'^2)\sum_j (g_j/\mu_j)(\mu_j^2+q^2)^{-1} , \quad (34)$$

where $q^2=(\mathbf{k}'-\mathbf{k})^2$. When we make a partial wave expansion of this, we get

$$v_l(k',k)=(1/4\pi)(k^2+k'^2)\sum_j (g_j/\mu_j)Q_l(y_j)/2kk' , \quad (35)$$

where y_i is the function of Eq. (25), but with μ replaced by μ_i.

Consider two limits: the case where one of the momentum arguments becomes large and the other is fixed, and where they become large together. In the first case, y is conveniently written

$$y_i=\frac{k}{2k'}+\frac{C_i}{k} , \quad (36)$$

where $C_i=(k'^2+\mu_i^2)/2k'$.

For $k\to\infty$, k' fixed, we require the limiting value[17] of Q_l,

$$Q_l(y_i)\to k^{-l-1}\left[1+\frac{2k'C_i^{-l-1}}{k^2}\right](k\to\infty, k' \text{ fixed})$$

$$\to k^{-l-1}+O(k^{-l-3}) . \quad (37)$$

In the second case, we take k and k' to infinity together. Then y becomes

$$y_i\to 1+\mu_i^2/2k^2 \quad (k=k'\to\infty) . \quad (38)$$

To analyze this behavior we need the asymptotic value[17] of Q_l in the neighborhood of its branch point at 1:

$$Q_l(1+\mu_i^2/k^2)\to -\gamma-\psi(l+1)-\ln\mu_i+\ln k \quad (k=k'\to\infty) , \quad (39)$$

where γ is the Euler constant and ψ is the digamma function.

For the first case, each term in the sum in Eq. (35) behaves like k^{-l}, a constant for S waves. For the second case, each term behaves like $\ln k$, diverging as k becomes large. In order to suppress these bad behaviors, the Paris group has chosen the coupling constants so that the sum satisfies

$$\sum_i g_i/\mu_i=0 . \quad (40)$$

This causes any i-independent terms in the asymptotic form of Q_l to cancel, including the k^{-l-1} term in the first case and the $\ln k$ term in the second. The result for k' fixed is a k^{-l-2} falloff; even the S wave vanishes. For $k=k'\to\infty$ the potential approaches a constant proportional to the sum $\sum_j g_j\ln\mu_j/\mu_j$.

Although these are well behaved in principle, in practice the momentum space potential matrix elements do not fall off until the cancellation begins to occur: at values of k which are 2 or 3 times larger than the largest μ_i. We therefore find matrix elements of the Paris potential continuing to grow until momenta of 20–30 fm^{-1} or higher. When solving the equation in momentum space this means that quadrature points at much larger momenta must be included, compared to the set used for the RSC potential. This difficulty translates into problems with the very short range behavior in coordinate space, where considerable care must also be employed.

This high momentum dependence makes the potential strongly off diagonal. For example, in the $^1S_0$ state, the matrix element $\langle k\,{}^1S_0 \mid v \mid k'\,{}^1S_0\rangle$ for k fixed at 1 fm^{-1} peaks at a value of $k'=22$ fm^{-1}. As can be seen from Fig. 2(a), for the S waves the worst behavior occurs for the diagonal matrix elements which go to a constant at infinity. This does not cause a serious problem in solving the equation for low momentum initial states, as can be seen from the discussion of convergence in the next section.

This behavior should serve as a warning to those who use this potential in nuclear matter calculations. The momenta of the most-favored intermediate states could be very high, even if the final G-matrix elements desired are to be evaluated for low momenta. Approximations to the Pauli operator may not be appropriate if they do not take this into account.

The P80 potential includes central, spin-orbit, tensor, and quadratic spin-orbit terms. The quadratic spin orbit is also a second-rank (reducible) tensor in spin, like the usual tensor force, but it does not couple state of different orbital angular momentum. The forms in momentum space, including matrix elements of the operators, are as follows (isospin indices have been suppressed):

$$v^{C}_{jll's}(k,k')=\delta_{ll'}\sum_j [g^a_j+g^b_j(k^2+k'^2)/\mu_j]A_{ll}(\mu_j)\ , \tag{41a}$$

$$v^{\mathrm{LS}}_{jll's}(k,k')=\delta_{ll'}\sum_j \{g^{\mathrm{LS}}_j[B_{ll}(\mu_j)-A_{ll}(\mu_j)]\}[j(j+1)-l(l+1)-s(s+1)]/6\ , \tag{41b}$$

$$v^{T}_{jll's}(k,k')=\delta_{s1}\sum_j g^T_j B_{ll'}(\mu_j)\left[(-1)^{j+1}2\sqrt{30}\sqrt{(2l+1)(2l'+1)}\begin{Bmatrix} l' & l & 2\\ 1 & 1 & j\end{Bmatrix}\begin{Bmatrix} l' & 2 & l\\ 0 & 0 & 0\end{Bmatrix}\right]\ , \tag{41c}$$

$$v^{S02}_{jll's}(k,k')=\delta_{ll'}\sum_j g^{S02}_j C_{ll}(\mu_j)l(l+1)\left[(4s-3)/3-s(-1)^{l+j}10(2l+1)\begin{Bmatrix} l & l & 2\\ 1 & 1 & j\end{Bmatrix}\begin{Bmatrix} l & l & 2\\ 1 & 1 & l\end{Bmatrix}\right]\ . \tag{41d}$$

The large curly braces denote $6j$ symbols. We follow the notation of Brink and Satchler.[23] $A_{ll'}$ and $B_{ll'}$ are defined in Eqs. (20) and (21) and $C_{ll}(\mu)$ is the ll matrix element [in the notation of Eq. (21)] of the function

$$C(x)=(1+3/x+3/x^2)e^{-x}/x^3\ . \tag{42}$$

Explicitly, one obtains

$$C_{00}(\mu)=0\ , \tag{43a}$$

$$C_{11}(\mu)=(k^2k'^2/3\mu^4)(-(1/4kk'\mu)\ln\{[1+(k+k')^2/\mu^2][1+(k-k')^2/\mu^2]\}+A_{33}/5-6A_{11}/5)\ , \tag{43b}$$

$$C_{ll}(\mu)=(k^2k'^2/\mu^4)[1/(2l+1)][A_{l-2\,l-2}/(2l-1)+A_{l+2\,l+2}/(2l+3)-(4l+2)A_{ll}/(2l-1)(2l+3)]\ . \tag{43c}$$

C. Comparison of the potentials

Both potentials are "realistic" in the sense that they produce good fits to the phase shifts up to 350 MeV and both include physical inputs assumed to be consistent with a nonrelativistic reduction of a relativistic meson exchange model. Thus, both have an OPEP tail, similar potentials in the TPEP region, smooth relative wave functions with an interior suppression, and no "extra" nodes or discontinuities at distances inside of 1 fm.[24] On the other hand, these two cases are about as different as potential models possessing these properties can be. The RSC potential is local in each partial wave, while the P80 is strongly nonlocal. When partial waves are added together and the potential matrix elements are considered in momentum space, the RSC has a slight nonlocality, while P80 is decidedly nonlocal. Thus, we expect them to be substantially different in their predictions at very high energies and very far from the energy shell. They illustrate the kind of "model dependence" which is permissible within the potential models of traditional nuclear physics.

We complete this section by comparing the momentum-space matrix elements of the two potentials. In addition to the usual spectroscopic notation we also label the states with the 3(4) integer strings slj ($sll'j$) for uncoupled (coupled) states. In Figs. 2 and 3 we show the matrix elements for the $^1S_0$ and $^3P_2$-$^3P_2$ states. Other states are qualitatively similar, with none of the states considered showing any significant similarities between RSC and P80. Notice that the largest matrix elements for RSC occur for both momenta less than about 10 fm^{-1}, while for P80 they are still growing at 20 fm^{-1}, especially along the diagonal. These figures confirm our expectations about the difference in the natural scales for the two potentials.

It seems extraordinary that two such strikingly different potentials can produce similar on-shell behavior as a function of energy, much less off-shell behaviors that remotely resemble each other. Nonetheless, we shall see below that the off-shell amplitudes are indeed quite similar.

IV. THE SOLUTION OF THE OFF-SHELL LS EQUATION

In this section we describe the method used to solve the fully-off-shell LS equation and discuss the various convergence tests applied.

A. Method of solution

The partial wave LS equation (9) presents two calculational problems. First, the principal value singularity corresponding to on-shell propagation must be handled numerically. Second, one must deal with the fact that the integral has an infinite range.

Choosing the principal value means that the integration is done excluding the singular point, and a limit is taken as the region of integration is allowed to approach the singularity symmetrically. This permits the cancellation of the positive and negative infinities on either side of the pole. Two methods may be employed to accomplish this. The singularity may be handled either by using a symmetric quadrature in the neighborhood of the pole (Sloan method),[25] or by explicitly subtracting off an integral which is identically zero but has the same pole structure as the term we are trying to calculate (Haftel-Tabakin method).[16] In the former case we have to worry that we will lose accuracy by having to subtract large numbers near the pole. In the latter we not only have to worry about the neighborhood of the pole, but that our quadra-

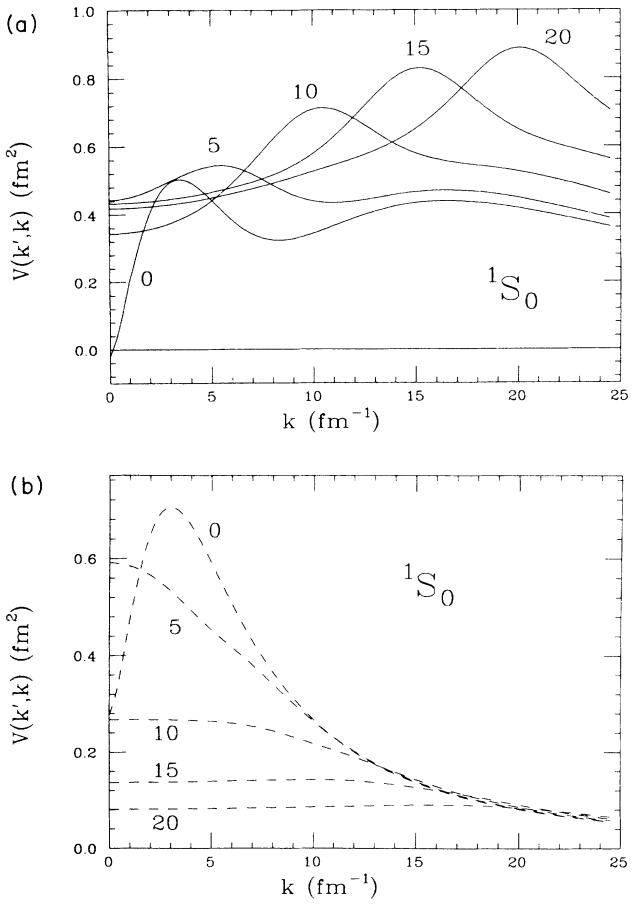

FIG. 2. Momentum space potential matrix elements $v_{000}(k',k)$ as a function of k parametrically in k'. The value of k' in fm^{-1} is placed near the relevant curve. (a) P80 (solid) and (b) RSC (dashed).

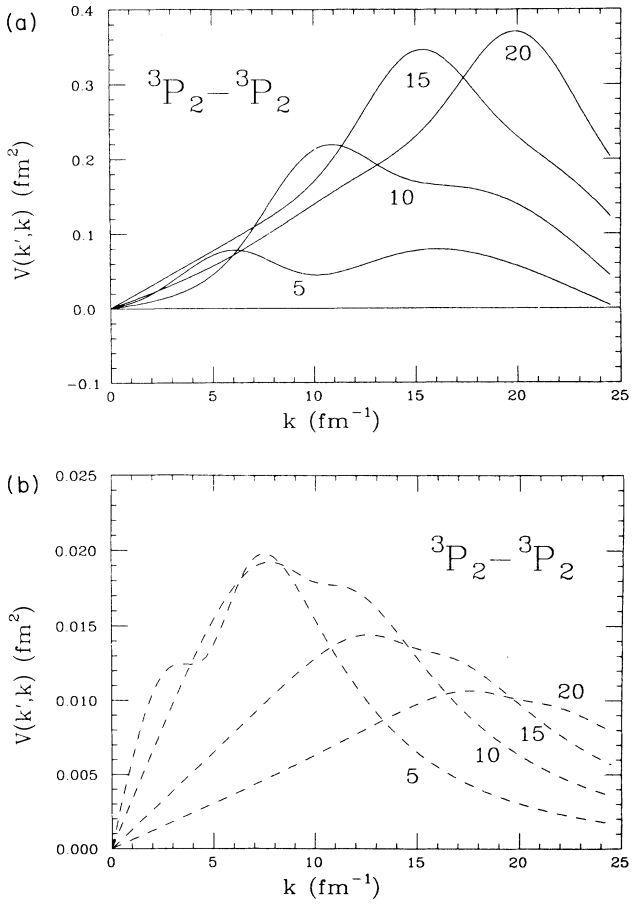

FIG. 3. Momentum space potential matrix elements $v_{1112}(k',k)$ as a function of k parametrically in k'. The value of k' in fm^{-1} is placed near the relevant curve. (a) P80 (solid) and (b) RSC (dashed).

ture is good enough over the entire region to give an accurate zero for the vanishing integral that has been subtracted.

We tried both methods and found the Sloan method to give a more accurate evaluation of the integral with a reasonable number of quadrature points. Our results indicate that, as Sloan suggested, one does not have to approach the pole so closely that accuracy problems begin to occur. We therefore simply select a symmetric bin of small width (ranging from 0.25 to 1.0 fm^{-1} half-width) about the on shell point and use a Gaussian quadrature in that bin with an even number of points. Our numerical studies indicate that 4 to 6 quadrature points in this bin provides sufficient accuracy.

In order to handle the infinite range of the integral, we go out to a cutoff momentum which is somewhat outside the region where the dominant contributions occur and use a Gauss-Laguerre rule for the integration region beyond that cutoff. Again, numerically we find that 5 to 7 points are adequate to describe this region numerically.

As a result of these choices, we are led to the following simple procedure. We divide the q integration in Eq. (9) or (12) into four bins: a symmetric bin of half-width Δ about the on-shell momentum p, a semi-infinite bin from a cutoff κ to ∞, a linear bin from 0 to $p-\Delta$, and a second linear bin from $p+\Delta$ to κ. The resulting equation takes the discrete form

$$k(q_i,q_j,p^2)=v(q_i,q_j)+\sum_m w_m(p^2) \times v(q_i,q_m)k(q_m,q_j,p^2) . \quad (44)$$

The weight function $w_m(p^2)$ includes the quadrature weights, the phase space factor q^2, the resolvent $(p^2-q^2)^{-1}$, and the numerical factor $4\mu/\pi$. We have suppressed the subscripts on k and v. If a tensor-coupled state is being described, k and v are both 2×2 matrices.

The on-shell point is included as a quadrature point with weight zero. This means it will be calculated as one of the values on the left-hand side of the equation, but it will not contribute to the sum on the right.

Equation (44) for the unknowns $k(q_i,q_j)$ is then solved using a standard linear equation solver. The T matrix is obtained from the K matrix by means of the algebraic equations (10) or (13). The values of the T ma-

trix for arbitrary values of its arguments are then obtained by a two dimensional fifth order Aitken interpolation.[17]

B. Comparison with other approaches

The two most common approaches for handling the singular denominator in the T matrix form of the LS equation are the K matrix method[12] and the Kowalski-Noyes method.[26] In the K-matrix method a supplementary quantity is introduced which solves the Lippman-Schwinger equation with the "$+i\epsilon$" prescription in the denominator replaced by the principal value. In the Kowalski-Noyes method, the equation is multiplied by a factor containing the ratio of potential matrix elements and a subtraction is performed to cancel the numerator at the pole. This method can only be used to calculate the half-shell T matrix. The fully-off-shell amplitude may then be constructed with a subtracted Low equation [see Eqs. (54) and (55) and the discussion in Sec. IV] first written down by Baranger, Giraud, Mukhopadhyay, and Sauer[27] (BGMS) and extended by Haftel[28] to include bound states.

The difficulty possessed by the Haftel-Tabakin method described above (i.e., maintaining accuracy for the whole integral, not just in the neighborhood of the singularity) applies to the Kowalski-Noyes approach as well. Experience with this equation indicates that a substantially larger number of quadrature points are required in order to obtain an accuracy comparable to the one we report here. In addition, this approach also suffers from the defect of requiring solution of the half-shell equation at many energies in order to produce fully-off-shell matrix elements at a single energy. A quadrature is also required for every off-shell matrix element constructed.

Our method has the advantage of dealing with the desired quantities directly in addition to being fast and efficient. The direct solution of the off-shell LS K-matrix equation and the associated Heitler equation to produce a fully-off-shell T matrix at a particular energy on a mesh of momenta adequate for interpolation takes less than 2 min of central processing unit time (CPU) on a CDC 7600 for 20 distinct nucleon-nucleon partial waves.

C. Convergence studies: The phase shifts

We carried out extensive studies of the convergence and the numerical stability with respect to the placement of the quadrature points of the off-shell LS equation for the K matrix for the two potentials both on and off shell.

A sample of the on-shell convergence results is shown in Table I. We display the phase shifts for the states $^1S_0$, $^3S_1$-$^3D_1$, $^3P_2$-$^3F_2$, $^1P_1$, and $^3D_2$ at a c.m. energy of 100 MeV. We use a value of Δ of 0.5 for the uncoupled states and 1.0 for the coupled states. For the RSC a value of $\kappa=10$ fm^{-1} is used for the 19 and 24 point quadratures, while for the 32 point rule κ is increased to 15. The three quadratures displayed have points distributed in the four bins by $19=3+4+8+4$, $24=5+6+8+5$, and $32=5+6+15+6$. For the P80 potential κ is taken to be 30 fm^{-1} and the quadrature points in each bin are divided up as follows: $21=3+4+10+4$, $24=3+4+12+5$, $30=3+6+15+6$, and $32=5+6+15+6$. All of the calculations reported here use a Gauss-Laguerre parameter of 1.0 fm^{-1}. These values were selected after extensive studies of the dependence of the results on the placement of the cutoffand the other binning parameters.

Our conclusion is that the on-shell phase shifts at lab energies between 25 and 350 MeV can be obtained to an accuracy of about 0.01° (usually better than 1 part of 1000) with 24 points for the RSC and 30 points for P80. For P80 we actually used 32 points since the stability of the interpolation routine near zero required more values.

The on-shell amplitudes produced were compared with the published versions of both Reid and Paris groups. Reid only gives his results to three significant figures (except for phase shifts greater than 1 rad, where he gives 4). For all the $T=0$ phase shifts we agree with his results to all places. For the coupling parameter ϵ_1 we agree to all figures given, except at the highest energies, where we agree to within 2% (about one-tenth of a degree). Our $T=1$ phase shifts are not precisely comparable with Reid's published values since he includes Coulomb amplitudes and we do not. Even after the extraction of the Coulomb amplitude from his results, his

TABLE I. Convergence of the phase shifts (in deg) for a sample of partial waves. The number of points in the quadrature rule (and the number of points in each bin) is, for RSC, (a)=19 (3 + 4 + 8 + 4), (b)=24 (5 + 6 + 8 + 5), (c)=32 (5 + 6 + 15 + 6); for P80, (d)=21 (3 + 4 + 10 + 4), (e)=24 (3 + 4 + 12 + 5), (f)=30 (3 + 6 + 15 + 6), (g)=32 (5 + 6 + 15 + 6). See text for ranges covered by each bin.

	$^1S_0$	$^3S_1$	$^3D_1$	ϵ_1	$^1P_1$	$^3P_2$	$^3F_2$	ϵ_2	$^3D_2$
					RSC				
(a)	5.784	18.64	−19.15	5.649	−25.18	15.86	1.263	−2.968	24.46
(b)	5.779	18.60	−19.11	5.668	−25.18	15.85	1.266	−2.966	24.49
(c)	5.777	18.58	−19.11	5.673	−25.18	15.85	1.266	−2.966	24.49
					P80				
(d)	5.242	19.68	−20.45	3.061	−21.84	16.16	1.092	−2.748	27.09
(e)	4.758	19.31	−20.47	3.181	−21.76	16.29	1.092	−2.743	27.15
(f)	4.813	19.26	−20.43	3.203	−21.75	16.32	1.096	−2.739	27.15
(g)	4.811	19.27	−20.43	3.200	−21.74	16.32	1.096	−2.739	27.15

nuclear phase shifts include the effects of second order Coulomb amplitude. These produce differences of about 2% between our phase shifts and his (up to as much as half a degree for the large phase shifts). For the Paris potential our $T=0$ phases agree with those published. A comparison with the calculations of Friar and collaborators[29] done in coordinate space without Coulomb potential shows excellent agreement with our $T=1$ phase shifts.

We have also compared the on-shell behavior predicted by the two potentials with the latest phase shift analysis of the Virginia Tech (VPI) group we had available (SP86).[30]

The phase shifts for RSC, P80, and VPI are plotted in Fig. 1. The agreement is good to excellent for most of the phases, though discrepancies of 2° or 3° are not uncommon. It should be noted that such discrepancies do not necessarily indicate failures in the potential models. Vinh Mau has stressed in his lecture in the Rho and Wilkerson volume[19] that his group fit the data directly and that their χ^2 values are comparable to those obtained by the VPI group in obtaining their energy-dependent phase shift fits. In producing such an energy-dependent phase shift, one must make certain assumptions as to the possible forms the energy dependence may take. These assumptions are not well documented or understood. The extraction of phase shifts at a single energy leads to error bars which are comparable to the differences seen in Fig. 1. Note also that Van Oers has pointed out[31] that potential model and phase shift predictions for some observables which have not been measured may differ substantially.

There are a few cases where the discrepancies between individual phase shifts are significant. The three predictions for the $^1P_1$ state look only qualitatively similar, while the singlet and triplet D_2 states show up to 20% variations, especially at the higher energies. The coupling parameter for the $J=1$ states also does not seem to be well determined. Klages has recently reported[10] that new data from Karlsruhe pin down the $^1P_1$ phase shift, which now agrees well with P80. The $J=1$ coupling parameter is still poorly determined at low energies. We will see in Sec. V that only the $^1P_1$ discrepancy corresponds to large off-shell differences.

D. Off-shell convergence

The fact that our calculations have converged for the on-shell value does not necessarily imply that we have comparable convergence for all off-shell values. We therefore also investigated the convergence of the off-shell matrix elements. This was done by comparing the curves for the $t_l(k',k;p^2)$ real and imaginary parts for an on-shell energy of 200 MeV (lab) as a function of k from 0 to 3.0 fm^{-1} parametrically for values of k' from 0 to 2.5 fm^{-1} in steps of 0.5 fm^{-1}. For the coupled states we compared the K matrices in the same way.

Our conclusion is that the number of points which yields good results for the phase shift also yields excellent results off shell in the ranges indicated. For the RSC calculations the results with 24 and 32 points were indistinguishable for all states. We used 24 points for all the calculations shown below. For P80 the results showed small differences between 24 and 30 point quadratures and none between 30 and 32. We used 32 points for all the calculations displayed.

A more cursory investigation of the off-shell convergence at other energies suggests that our off-shell amplitudes are also well converged at all lab energies ranging from 100 to 350 MeV. At 50 MeV some changes in the off-shell amplitudes were observed at high momenta (k and $k' \gtrsim 2.0$ fm^{-1}), while at 20 MeV significant variations were found even at low momenta, even though the on-shell results were still accurate at both energies.

It is clear from these results that off-shell convergence cannot be inferred from on-shell convergence. The accuracy of the specific matrix elements desired must be investigated directly.

V. OFF-SHELL COMPARISON OF RSC AND P80

In order to compare the off-shell amplitudes produced by the RSC and P80 potentials, we have examined the region of lab energies ranging from 100 to 350 MeV by considering the off-shell K matrices $k_l(k',k;p^2)$ as functions of k from 0 to 3.0 fm^{-1} parametrically in k' for values of k' ranging from 0 to 2.5 fm^{-1} in steps of 0.5 fm^{-1}. Since a detailed comparison involves hundreds of curves (14 states, four energies, five k' curves, and two models), we cannot display them all here. Rather, we will display a comparison of the K matrices produced by the RSC and P80 potentials for each partial wave at 200 MeV. The variation with energy will be discussed in the text. For some of the states we have also considered the behavior at lab energies down to 20 and up to 400 MeV.

The relation between the K matrices shown and the T matrices actually used in calculations is simple [Eqs. (10) and (13)]. For most of the states considered, the structures of the momentum dependence is very similar for the K and the T matrices. This is particularly true in the weaker states.

A. $J=0$ states

$^1S_0(000)$. The off-shell K-matrix elements for this state are shown in Fig. 4. In this and in the remaining figures, the P80 curves are drawn as solid lines and the RSC as dashes. The structure of this figure is similar at all energies from 20 to 400 MeV. The magnitudes are very large at low energies due to the antibound-state pole and fall rapidly until about 100 MeV, where they stabilize. The energy dependence in the 100–350 MeV region is slight. This is exemplified by the energy dependence of the values of $k_{000}(0,0;p^2)$ displayed in Fig. 5. The variation between 100 and 350 MeV is only about 15%.

In this (and succeeding figures displaying the energy dependence) the points actually calculated are marked with a cross. The curves are interpolations provided by the plotting program.

At energies below about 200 MeV the k' curves cross (or nearly so) in the neighborhood of $k=(1.85+0.005E)$ fm^{-1}. As the energy increases this point moves out and becomes fuzzier, being replaced at the higher energies by a narrowing.

The RSC and P80 amplitudes agree to better than 20% over the entire range of energy and momentum con-

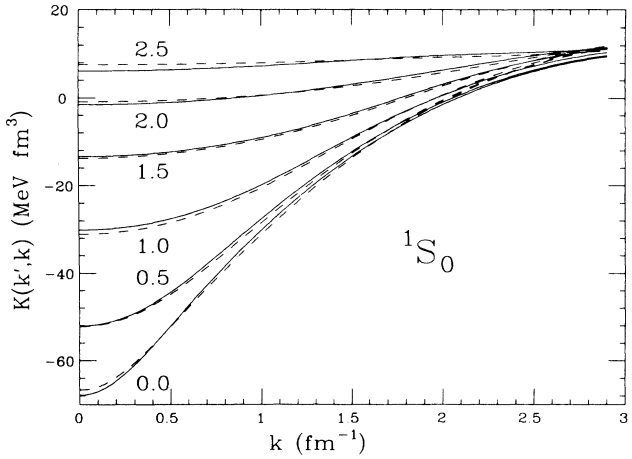

FIG. 4. Fully-off-shell K-matrix elements $k_{000}(k',k;E)$ for $E=200$ MeV (lab) as a function of k parametrically in k' for P80 (solid) and RSC (dashed). The value of k' in fm^{-1} is placed near the relevant curve.

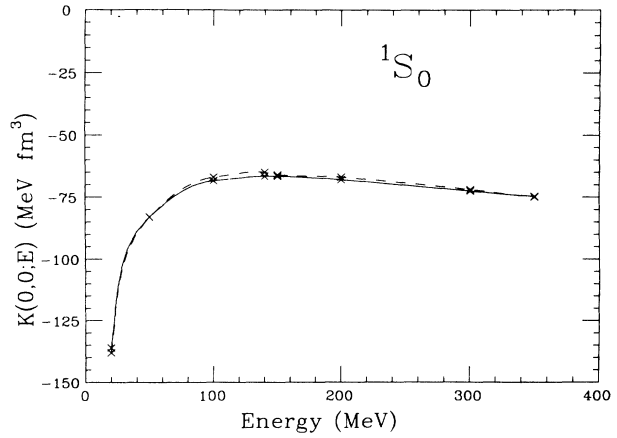

FIG. 5. Energy dependence of the K-matrix element $k_{000}(0,0;E)$ as a function of lab energy.

sidered. For k and $k' \leq 2.0$ fm^{-1} the agreement between P80 and RSC is quantitatively excellent, i.e., better than 5% everywhere except where the value of the amplitude is small in association with passing through zero.

In general, we will quote percentage discrepancies in terms of percentages of the larger values of the amplitudes displayed on the graphs. When the amplitude crosses zero, the percentage differences may become very large. We will henceforth drop the warning phrase "except when the amplitude becomes small." If one is interested in an integral over a broad range of momenta, our quoted percentages then represent realistic ranges of variability. If a single matrix element or a very narrow range is required, the differences can be much greater due to the magnifying effect of small values.

$^3P_0(110)$. The off-shell amplitudes for this state are displayed in Fig. 6. The scale of these amplitudes remains the same from 20 to 400 MeV. Below 50 MeV a second peak appears in the k' curves inside the 3 fm^{-1}. The qualitative structure is very stable from 100 to 350 MeV, with the maximum values of the peaks changing by less than 30% over the entire range.

The P80 and RSC amplitudes in this state are qualitatively similar over the entire range examined. They agree to better than 10% for momenta k and $k' \leq 1.5$ fm^{-1}. As the momenta increase, the discrepancies grow slowly to a maximum of about 15% when $k=3$ fm^{-1} and $k'=2.5$ fm^{-1}.

B. $J=1$ uncoupled states

$^3P_1(111)$. The off-shell amplitudes for P80 and RSC at 200 MeV are shown in Fig. 7. From 50 to 350 MeV each k' curve has a single peak which moves outward in k as k' increases. The energy dependence is fairly small, with the heights of the peaks changing by about 20% between 50 and 350 MeV. This behavior is illustrated in

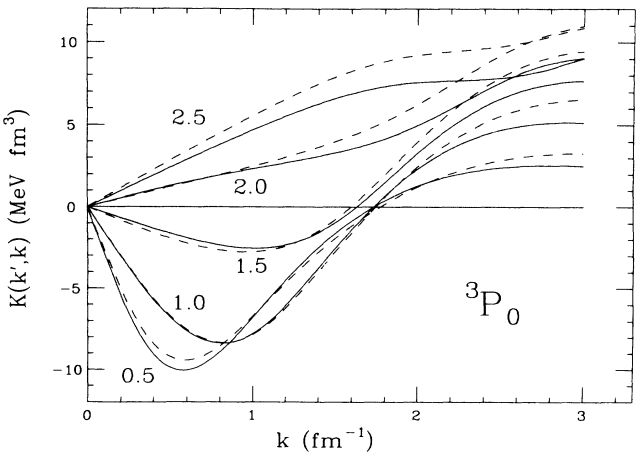

FIG. 6. Fully-off-shell K-matrix elements $k_{110}(k',k;E)$ for $E=200$ MeV (lab) as a function of k parametrically in k' for P80 (solid) and RSC (dashed). The value of k' in fm^{-1} is placed near the relevant curve.

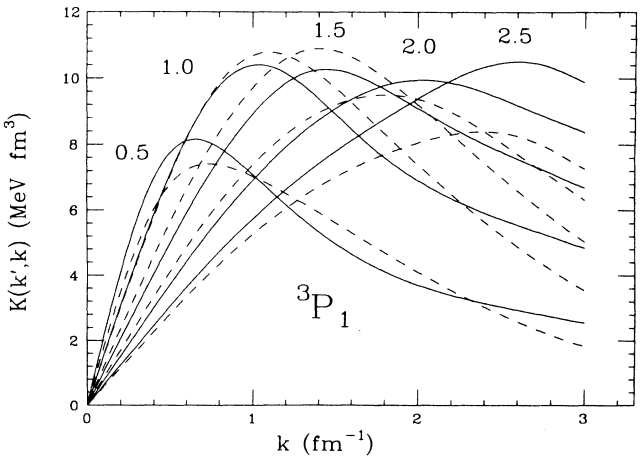

FIG. 7. Fully-off-shell K-matrix elements $k_{111}(k',k;E)$ for $E=200$ MeV (lab) as a function of k parametrically in k' for P80 (solid) and RSC (dashed). The value of k' in fm^{-1} is placed near the relevant curve.

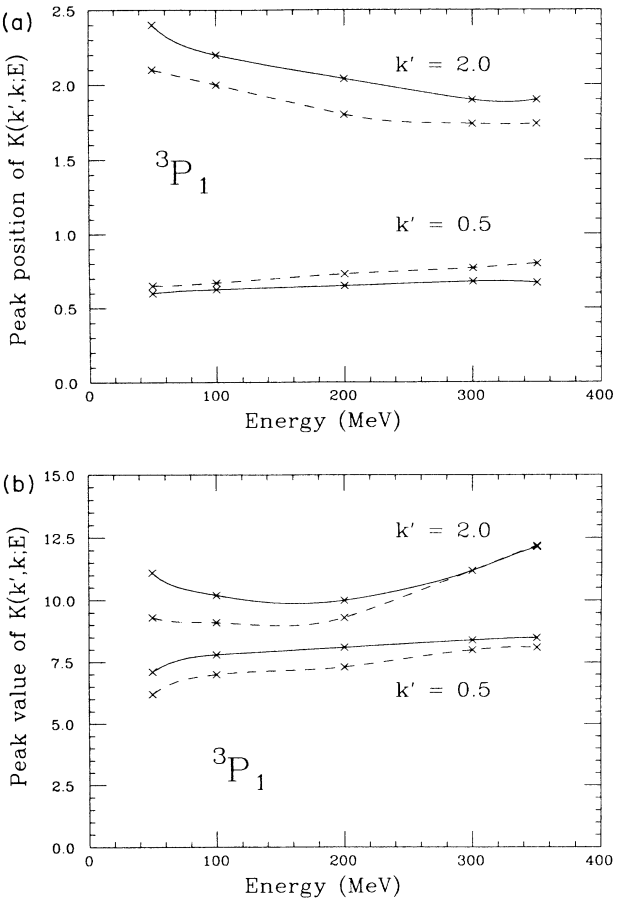

FIG. 8. Energy dependence of the peak in the function $f(k)=k_{111}(k',k;E)$ for $k'=0.5$ and 2.0 fm^{-1}. (a) Position of the peak in k (fm^{-1}); (b) value at the peak (MeV fm^3).

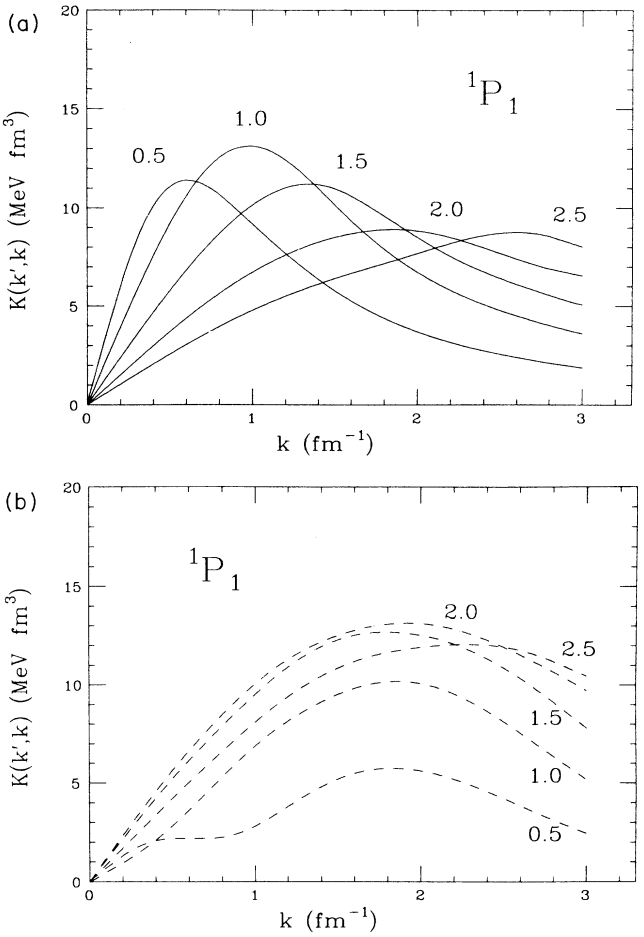

FIG. 9. Fully-off-shell K-matrix elements $k_{011}(k',k;E)$ for $E=200$ MeV (lab) as a function of k parametrically in k' for (a) P80 (solid) and (b) RSC (dashed). The value of k' in fm^{-1} is placed near the relevant curve.

Fig. 8, where we have plotted (a) the position in k' and (b) the value of the peak in the $k'=0.5$ and 2.0 fm^{-1} curves.

Again, the P80 and RSC amplitudes are qualitatively similar (i.e., agree to better than 10%) in the energy range from 50 to 350 MeV for k and $k' \lesssim 2.0$ fm^{-1}, with the discrepancies being slightly higher ($\lesssim 20\%$) at higher momenta and at 350 MeV.

$^1P_1(011)$. The $^1P_1$ state is the only one we have found in which P80 and RSC differ substantially. The differences are so large that plotting them on the same graph would result in a very confusing figure. We have therefore plotted the P80 and RSC amplitudes separately in Figs. 9(a) and 9(b). The P80 amplitudes have k' curves which peak near the diagonal value, $k=k'$. The shapes remain similar as a function of energy from 100 to 350 MeV but grow in magnitude fairly substantially. For example, the value at the peak of the $k'=1.5$ fm^{-1} curve grows by more than 50% in that energy range.

The RSC amplitudes tend to have broader peaks in the k' curves than do the P80 ones and they tend to be farther out—mostly in the neighborhood of 2 fm^{-1}. These also have a fairly strong energy dependence with the heights of the k' peaks growing by 30–50 % as the energy grows from 100 to 350 MeV.

C. $J=2$ uncoupled states

$^1D_2(022)$. The P80 and RSC amplitudes for this state are shown in Fig. 12. For 100 to 400 MeV the k' curves all form a single broad peak between $k=0$ and 3 fm^{-1}. Below 100 MeV the first nonzero k' curve ($k'=0.5$ fm^{-1}) develops a dip as well. Above 100 MeV the energy dependence is small. The peak value of the $k'=2$ fm^{-1} curve falls by about 10% as the energy grows from 100 to 400 MeV. Most differences are less than that.

P80 and RSC are very close in this state, with most discrepancies being less than 10%. There is some difference in how the $k'=2.5$ fm^{-1} curve heads downward from its peak, which leads to differences for $k>2.5$ fm^{-1} for $E \geq 100$ MeV.

$^3D_2(122)$. The P80 and RSC amplitudes for this state are shown in Fig. 10. As in the singlet case, most of the k' curves have a single broad peak in the $k=0$ to 3 fm^{-1} range, with the exception being low k' curves at energies below 100 MeV. The energy dependence is fairly strong, as is illustrated by the energy variation of the maximum value in the $k'=1.5$ fm^{-1} at all energies investigated (Fig. 11).

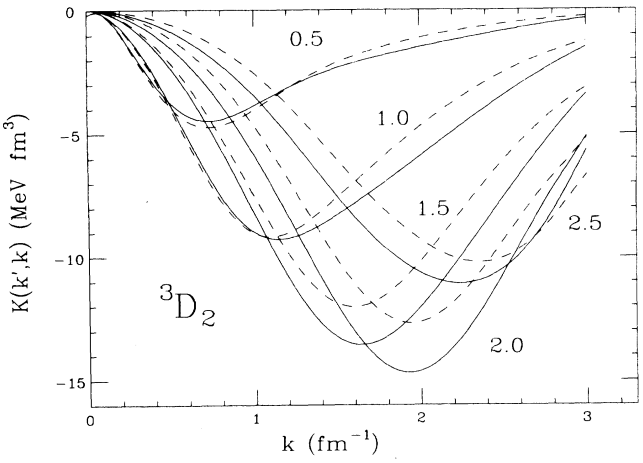

FIG. 10. Fully-off-shell K-matrix elements $k_{122}(k',k;E)$ for $E=200$ MeV (lab) as a function of k parametrically in k' for P80 (solid) and RSC (dashed). The value of k' in fm^{-1} is placed near the relevant curve.

The agreement between P80 and RSC is very good (better than 15%) in the energy range from 100 to 350 MeV.

D. $J=1$ coupled state

$^3S_1$-$^3S_1$(1001). The ^3S-^3S block of the $J=1$ 2×2 K matrix has the largest matrix elements of any state at low energies (below about 50 MeV). Its values falls rapidly until about 200 MeV, after which it settles down to nearly a constant. The momentum structure is similar at each energy and is similar to that of the $^1S_0$. The matrix elements for P80 and RSC are shown at 200 MeV in Fig. 13.

RSC and P80 agree quite closely over the energy range from 50 to 400 MeV. The differences are less than 5% for k and $k'\leq 2.0$ fm^{-1} for $E\leq 200$ MeV and begin to grow slightly larger above that. At 300 MeV and above the differences are 15–20% for large momenta. The $K'=2$ fm^{-1} curves agree almost perfectly at these energies, with discrepancies increasing for higher momenta. The energy dependence of the value of $k_{1001}(0,0;p^2)$ is shown in Fig. 14.

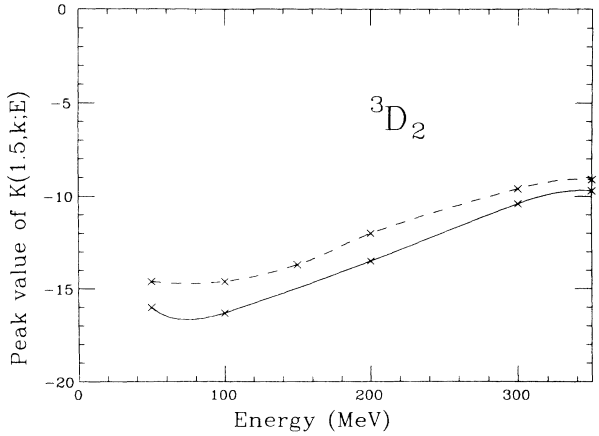

FIG. 11. Energy dependence of the value at the peak in the function $f(k)=k_{122}(k',k;E)$ for $k'=1.5$ fm^{-1}. The peak occurs close to $k=1.5$ fm^{-1} for all energies considered.

$^3S_1$-$^3D_1$(1201-1021). The off-diagonal block $k_{1021}(k',k;p^2)$ of the $j=1$ K matrix is shown at 200 MeV in Fig. 15. The energy dependence from 200 to 400 MeV is slow, with the peaks moving out slightly and decreasing in magnitude somewhat. As the energy drops below 200 MeV the peaks grow and move inward, with the higher k' curves beginning to develop a minimum at high k values. The energy dependence of the peak in the k curve $k_{1021}(0,k;p^2)$ as a function of energy is shown in Fig. 16.

At 100 MeV and above the P80 and RSC amplitudes agree to better than 10% everywhere with better than 5% more typical. At 50 MeV the agreement is still good (better than 15%) for $k'\leq 2.5$ fm^{-1} and $k\lesssim 2.0$ fm^{-1}.

$^3D_1$-$^3D_1$(1221). The P80 and RSC amplitudes at 200

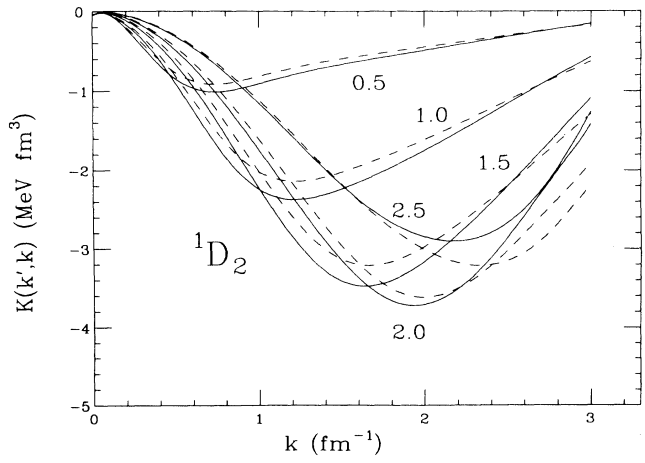

FIG. 12. Fully-off-shell K matrix elements $k_{022}(k',k;E)$ for $E=200$ MeV (lab) as a function of k parametrically in k' for P80 (solid) and RSC (dashed). The value of k' in fm^{-1} is placed near the relevant curve.

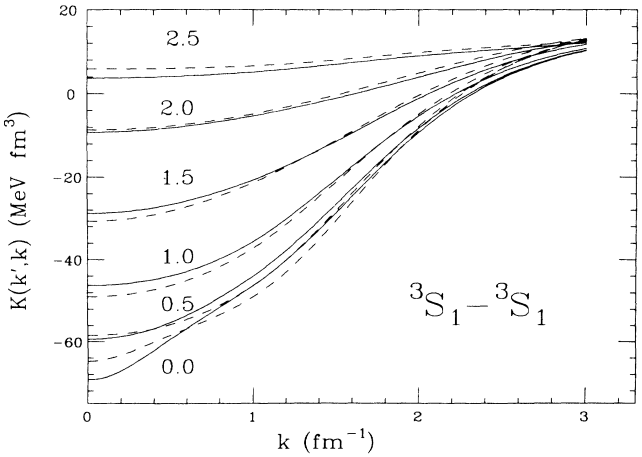

FIG. 13. Fully-off-shell K matrix elements $k_{1001}(k',k;E)$ for $E=200$ MeV (lab) as a function of k parametrically in k' for P80 (solid) and RSC (dashed). The value of k' in fm^{-1} is placed near the relevant curve.

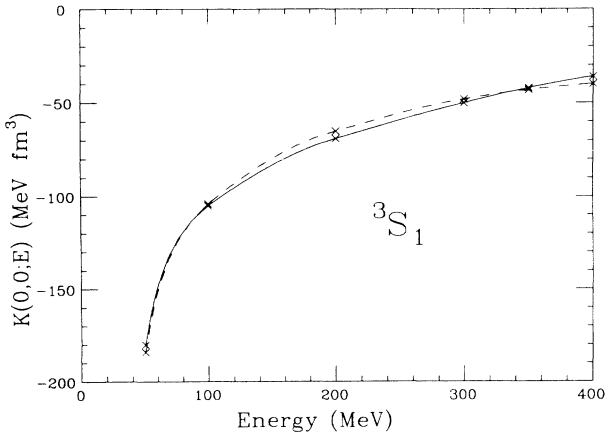

FIG. 14. Energy dependence of the K-matrix element $k_{1001}(0,0;E)$ as a function of lab energy.

MeV are shown in Fig. 17. The shapes of the curves are similar at other energies, except at 50 MeV, where the high k' curves have a zero in the k region examined. There is a strong energy dependence up to 100 MeV which weakens substantially from 200 to 400 MeV. P80 and RSC agree very well between 100 and 400 MeV. The agreement is better than 20% everywhere and usually better than 5%.

E. $J=2$ coupled states

$^3P_2$-$^3P_2$(1112). The P80 and RSC amplitudes for the 1112 block of the $J=2$ coupled K matrix are shown in Fig. 18. The energy dependence of these amplitudes is very small over the entire range from 50 to 400 MeV, with an overall change of magnitude of only about 20%. The two models, agree very well (to better than 5%) at all the energies considered.

$^3F_2$-$^3F_2$(1132-1312). The 1132 amplitudes are shown in Fig. 19. The energy dependence of these amplitudes

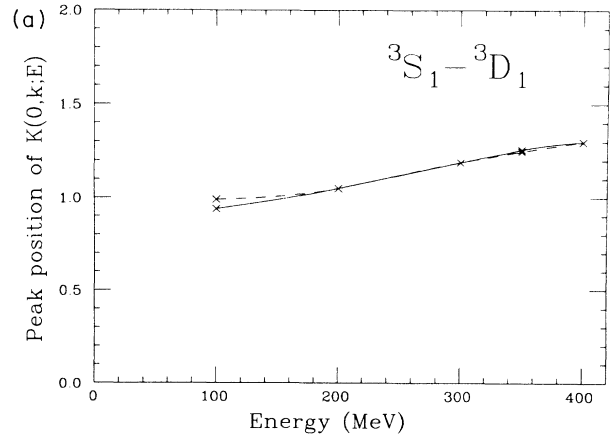

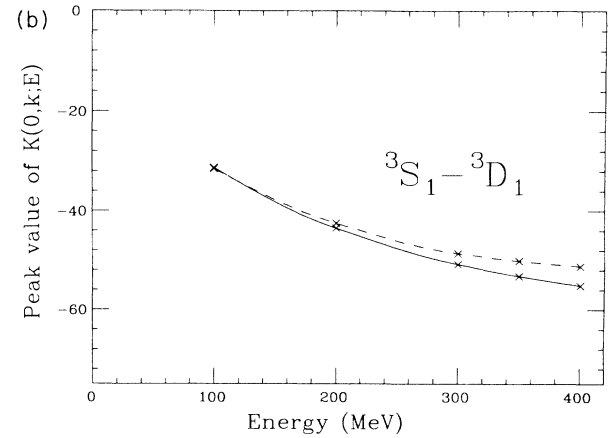

FIG. 16. Energy dependence of the peak in the function $f(k)=k_{1021}(k',k;E)$ for $k'=0$ fm^{-1}. (a) Position of the peak in k (fm^{-1}); (b) value at the peak (MeV fm^3).

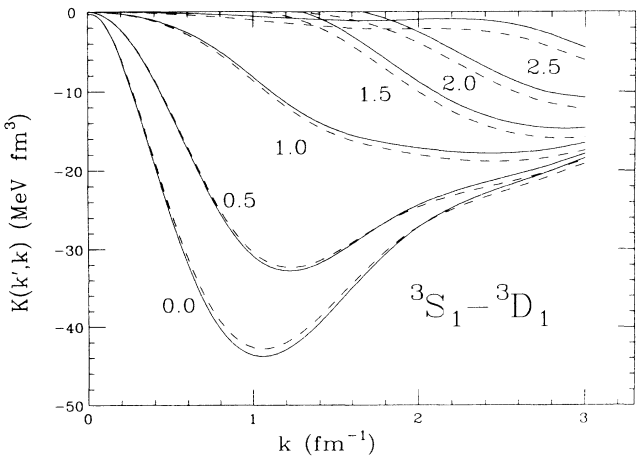

FIG. 15. Fully-off-shell K-matrix elements $k_{1021}(k',k;E)$ for $E=200$ MeV (lab) as a function of k parametrically in k' for P80 (solid) and RSC (dashed). The value of k' in fm^{-1} is placed near the relevant curve.

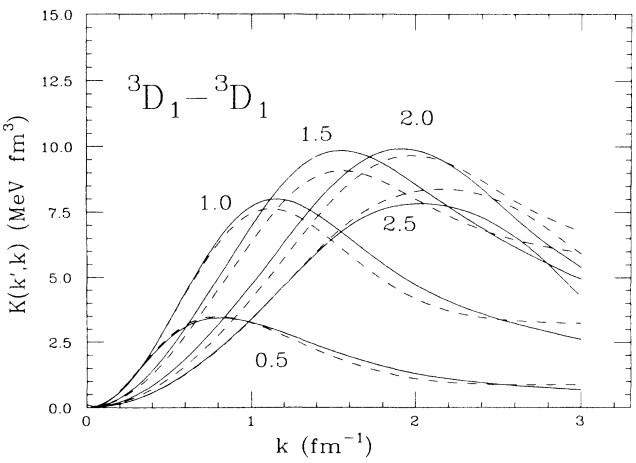

FIG. 17. Fully-off-shell K-matrix elements $k_{1221}(k',k;E)$ for $E=200$ MeV (lab) as a function of k parametrically in k' for P80 (solid) and RSC (dashed). The value of k' in fm^{-1} is placed near the relevant curve.

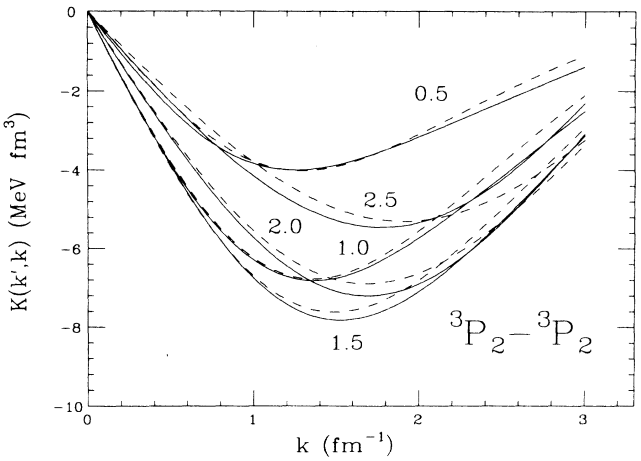

FIG. 18. Fully-off-shell K-matrix elements $k_{1112}(k',k;E)$ for $E=200$ MeV (lab) as a function of k parametrically in k' for P80 (solid) and RSC (dashed). The value of k' in fm^{-1} is placed near the relevant curve.

is again small, in the range 50–400 MeV. Figure 20 displays the movement of the peak height and position in the $k'=1.0$ fm^{-1} curve. RSC and P80 agree to within better than 10% everywhere.

$^3F_2$-$^3F_2$(1332). The amplitudes for this block are shown in Fig. 21. P80 and RSC agree here only for low values of k and k' (less than about 1.0 fm^{-1}). Above that they begin to differ substantially. As k' increases past 1.5 fm^{-1} the curve changes character, moving from negative to positive. P80 amplitudes do this more rapidly than RSC amplitudes and the former wind up more positive at large k. This effect is stronger for higher energies.

F. Discussion

The most striking observation about the set of amplitudes displayed is the close similarity between the two models in almost all states. This is particularly notable

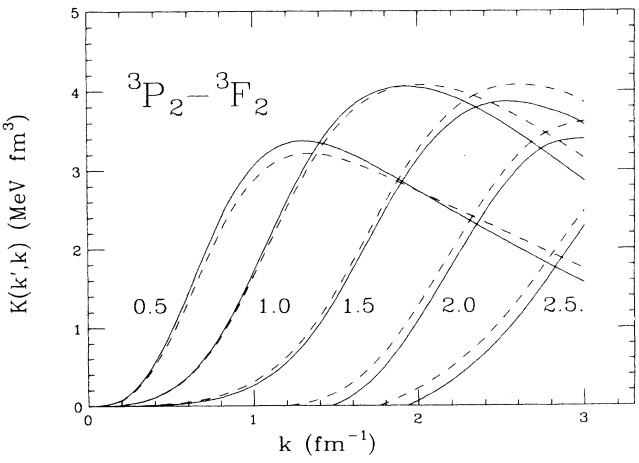

FIG. 19. Fully-off-shell K-matrix elements $k_{1132}(k',k;E)$ for $E=200$ MeV (lab) as a function of k parametrically in k' for P80 (solid) and RSC (dashed). The value of k' in fm^{-1} is placed near the relevant curve.

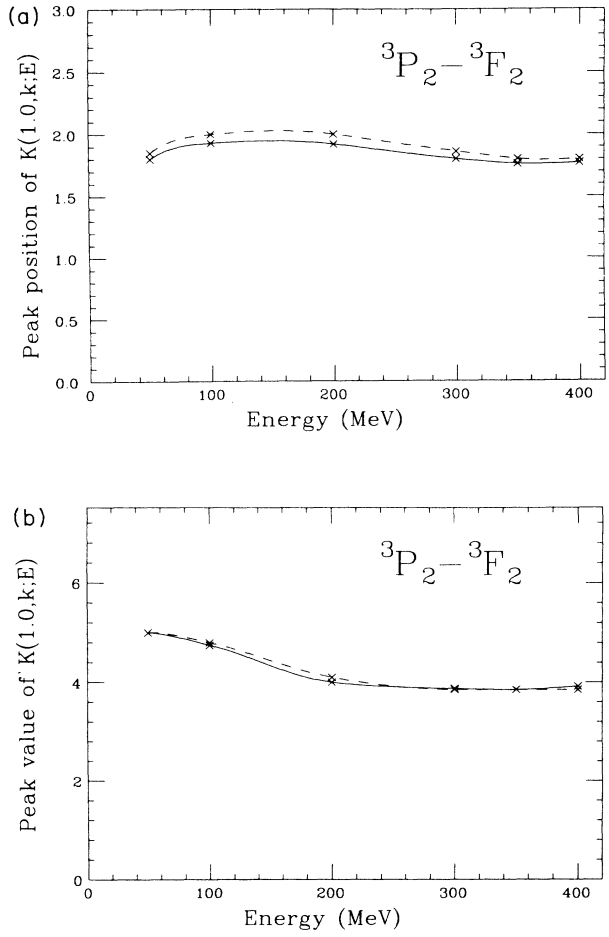

FIG. 20. Energy dependence of the peak in the function $f(k)=k_{1132}(k',k;E)$ for $k'=1.0$ fm^{-1}. (a) Position of the peak in k (fm^{-1}); (b) value at the peak (MeV fm^3).

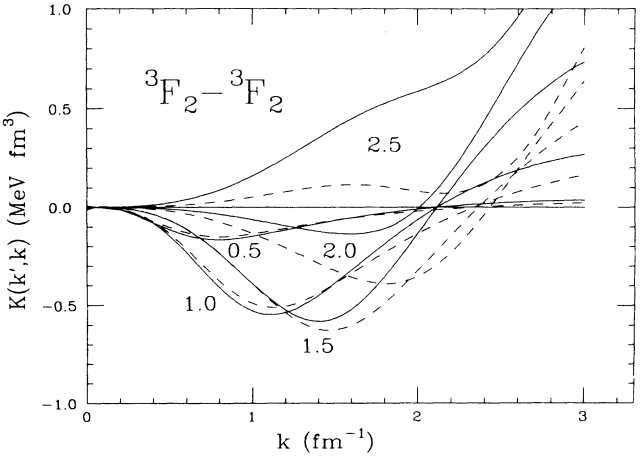

FIG. 21. Fully-off-shell K-matrix elements $k_{1332}(k',k;E)$ for $E=200$ MeV (lab) as a function of k parametrically in k' for P80 (solid) and RSC (dashed). The value of k' in fm^{-1} is placed near the relevant curve.

given that the potential matrix elements in momentum space fail to be even qualitatively similar in any of the states examined. Despite this, the model amplitudes agree to within better than 10% or 20% for almost all states, energies, and momenta considered. The agreements are particularly good for $k,k' \leq 1.5$ fm^{-1}.

The two exceptions to these statements are the $^1P_1$ state and the $^3F_2$-$^3F_2$ block of the $J=2$ coupled state. The P state discrepancy is signaled by the qualitative agreement between the phase shifts in the two models [Fig. 1(c)]. The $^3F_2$ phase shifts [Fig. 1(f)] display a qualitative difference in character in the way they behave at high energy.

Surprisingly, quantitative disagreements such as displayed by the ϵ_1 parameter [Fig. 1 (g)] or the uncoupled D states [Figs. 1(d) and 1(e)] do not signal off-shell divergences between the models. The off-shell discrepancies in these cases are less than or comparable to the on-shell differences.

VI. ANALYSIS OF RESULTS

As a result of the calculations reported above, we conclude that the off-shell matrix elements of two very different potential models are very similar over a significant range of momenta and energies. Compelling conclusions cannot be drawn from the comparison of only two models (especially without a detailed analysis of the most sophisticated meson exchange potentials[9]). Nonetheless, in this section we consider some speculations as to how this result might be understood and what some implications might be for the analysis of many-particle properties in the framework of nonrelativistic nuclear physics.

We discuss how information about the two-nucleon system is stored in the half and off-shell T matrices. Finally, we discuss the implications of our results for some specific many-body calculations.

A. The validity of potential models

In the traditional model of nuclear physics we assume that nuclei can be described as consisting of nonrelativistic nucleons interacting via energy-independent (possibly nonlocal) two-body potentials. The two-body potentials are constructed, as described above, by a mixture of meson theory and phenomenology.

A nuclear system has a wide variety of properties, and what it looks like depends to a certain extent of the character and energy of our probe. The bulk of traditional nuclear physics deals with low energy properties such as binding energies, spectroscopic factors, and reaction rates. We will concentrate on such properties here.

At energies for which there is substantial pion production, a real, energy-independent potential is inadequate to describe the physics taking place. We therefore do not expect a potential model to suffice above about 350 Mev. The limitations in relative momenta are less clear, but 350 MeV corresponds to an on-shell relative momentum of about 4.5 fm^{-1}. Momentum transfers this high can be produced on shell when the initial and final momenta are half this size or about 2.5 fm^{-1}. Above momentum transfers of about 4 or 5 fm^{-1}, many calculations show that contributions from mesons and deltas are important even for a system as simple as the three-nucleon bound state.[32]

From our studies of the two potentials it is clear that the potential matrix elements are poorly determined even at low energy and momentum. However, our results suggest that we may be able to get reasonably well defined nonrelativistic amplitudes in this regime.

We therefore define scattering amplitudes at projectile lab energies below 350 MeV and relative nucleon-nucleon momenta below 2.5 fm^{-1} as in *the potential regime*. We suspect that it is only within this regime and only when we work with amplitudes that traditional nonrelativistic nucleons-only nuclear physics might be expected to work without the need for a careful evaluation of the dynamic contribution of delta and mesonic degrees of freedom.

Note that the matrix elements of the potential are required outside the potential regime in order to calculate amplitudes inside the potential regime. While individual potential matrix elements outside this regime may not be meaningful, they are required to yield fits to the on-shell data at low energies and momenta and to respect the long range constraints of meson theory. They are therefore constrained in a distinctly non-obvious way.

We must require that our method of constructing potentials contains enough input physics that the resulting theory is well determined. To construct a potential we use some meson theory and then fit many parameters to the two-body data. Different individuals and groups carrying out the procedure in distinct and idiosyncratic ways have obtained potentials which appear to be widely different. This casts doubt on whether the whole approach makes any sense.

However, the results we described in the preceding section indicate that the fully-off-shell T-matrix elements in the potential regime are much better determined than we might have guessed by comparing the potentials directly, either in coordinate or in momentum space. This could mean that the physics information that is common to all realistic potential models is sufficient to adequately determine off-shell amplitudes in the potential regime. If this information is adequate for the calculation of any many-body properties, it may mean that at least certain aspects of the nonrelativistic model are well defined.

In order to understand how information about two-nucleon physics determines the off-shell amplitudes, we consider first the half-shell amplitudes.

B. Two-body information and the half-shell T matrix

If the potential is local and energy independent, then it is a function of only one (vector) variable. We might then expect that all the information about the potential is contained in another function of one (vector) variable, the half-shell T matrix with the energy held fixed and the off-shell momentum allowed to roam. This is indeed the case since the scattering wave function at a given energy is completely determined by the half-shell T matrix at that energy through the equation[12]

$$\langle \mathbf{k}' \mid \psi_{\mathbf{k}} \rangle = \delta(\mathbf{k}'-\mathbf{k}) + (E_k^+ - E_{k'})^{-1} \langle \mathbf{k}' \mid T(E_k^+) \mid \mathbf{k} \rangle \quad (45)$$

for the component of the scattering wave function in the momentum representation. Upon Fourier transforming to coordinate space, the potential can then be, in principle, extracted from the Schrödinger equation in the form

$$V(\mathbf{r})=[(E_k-H_0)\psi_{\mathbf{k}}(\mathbf{r})]/\psi_{\mathbf{k}}(\mathbf{r}) . \tag{46}$$

This is not particularly convenient in practice, since the half-shell T matrix must be very well known very far off shell to construct the wave function. The information contained in the half-shell T matrix is more conveniently expressed using the form[12]

$$\langle \mathbf{k}' \mid T(E_k^+) \mid \mathbf{k} \rangle = \langle \mathbf{k}' \mid V \mid \psi_{\mathbf{k}} \rangle . \tag{47}$$

This shows that the half-shell T matrix is the Fourier transform of the coordinate space function $\langle \mathbf{r} \mid V \mid \psi_{\mathbf{k}} \rangle$ [i.e., $V(\mathbf{r})\psi_{\mathbf{k}}(\mathbf{r})$ for a local potential], so it is a reasonably direct measure of the wave function inside the range of the potential. This makes the half-shell amplitudes of particular importance in understanding the relation between physical constraints on the relative two-body wave function and the off-shell amplitudes.

The information in the half-shell T can be understood in greater detail when a partial-wave expansion is made. In addition to the partial-wave decompositions (6), we require the partial-wave expansion of the wave functions

$$\langle \mathbf{r} \mid \mathbf{k} \rangle = \sum Y_{lm}(\Omega_r)^* i^l j_l(kr) Y_{lm}(\Omega) , \tag{48a}$$

$$\langle \mathbf{r} \mid \psi_{\mathbf{k}} \rangle = \sum Y_{lm}(\Omega_r)^* i^l \psi_l(k;r) Y_{lm}(\Omega) . \tag{48b}$$

We have ignored tensor forces for simplicity, but have not assumed that the potential is local. These expansions yield the expression for the half-shell partial-wave T-matrix element

$$t_l(k',k;k^2)= \int\int r^2 dr\, r'^2 dr' j_l(kr) v_l(r,r') \psi_l(k;r') . \tag{49}$$

Although this appears to depend specifically on the potential, we know from Eq. (45) that the half-shell T only depends on the wave function. To see this in partial-wave form, we use the (partial-wave) Schrödinger equation to replace $V\psi$ by $(E-H_0)\psi$. If we were to insist that the potential were local, then, as we have seen, it could be extracted from the wave function. However, if we permit nonlocal potentials, then $V\psi$ is no longer proportional to ψ and we cannot extract V by using Eq. (46). This means that different potentials may lead to the same scattering wave function at a given energy and therefore to the same half-shell T matrix at that energy.

A useful expression of this can be obtained by integrating the $H_0\psi$ term by parts. This cannot be done directly, because an indeterminate surface term would be picked up at infinity. We can do it if we use the relation

$$(E-h_0)\psi_l=(E-h_0)(\psi_l-v_l) , \tag{50}$$

where $v_l(kr)$ is the phase-shifted free wave function

$$v_l(kr)=h_l^{(-)}(kr)-e^{2i\delta_l(k)}h_l^{(+)}(kr) . \tag{51}$$

We write

$$\Delta_l(k;r)=e^{-i\delta_l(k)}kr[\psi_l(k;r)-v_l(kr)] \tag{52}$$

for the difference function. This is the scattering state analog of the defect function studied in nuclear matter. It is real and goes to zero outside the range of the potential where the wave function attains its asymptotic form.

The expression (49) with $V\psi$ replaced by $(E-H_0)\Delta$ may now be integrated by parts. The result is

$$t_l(k',k;k^2)= (k'/k)^l t_l(k) - e^{i\delta_l(k)}[(k'^2-k^2)/k'k] \times \int dr\, u_l(k'r)\Delta_l(k;r) , \tag{53}$$

where $t_l(k)$ is the on-shell partial-wave T matrix, $t_l(k,k;k^2)$, and $u_l(x)$ is the Ricatti-Bessel function, $xj_l(x)$. Since on shell $k'^2=k^2$, this equation shows that the behavior of the half-shell T matrix away from the on-shell point is controlled by the Fourier transform of the difference function. Equation (53) was first found by Fulton and Shwed[33] and was used in Ref. 6 to analyze the sensitivity of the off-shell behavior to the interior wave function. From that work we learn that the half-shell T matrix within about 1–2 fm^{-1} of the on-shell point is well determined by the phase shift, the range and strength of the long and medium range attractions, the fact of short range repulsion, and the smoothness of the wave function.

C. Information in the fully-off-shell T matrix

The change of the scattering wave function from one energy to another tells us something about the nonlocality or the energy dependence of the potential. For an energy-independent potential, the fully-off-shell T matrix may be expressed in terms of half-shell T matrices.[27] This means that the fully-off-shell T matrices contain no more information than do the half-shell ones, but the way the information is distributed may be quite different.

The relation between the full and half-off-shell T matrices may be obtained by writing the partial-wave version of Eq. (1) for the half-shell energy E_k and putting in complete sets at the resolvent G. The result for an uncoupled partial wave without a bound state is

$$t_l(k',k;p^2)=t_l(k',k;k^2)+2\mu \int q^2 dq\, t_l(k',q;q^2) t_l^*(k,q;q^2)[(p^2-q^2+i\epsilon)^{-1}-(k^2-q^2+i\epsilon)^{-1}] . \tag{54}$$

(More general results may be found in Ref. 28.) We refer to this (and the analogous equations in the presence of coupled and bound states) as the BGMS equation.[28]

The BGMS argument may be carried a step further to yield a stronger result. If instead of a single subtraction on the Low equation, we perform two, we can demonstrate the relationship[34]

$$t_l(p,k;\lambda^2)=\left[\frac{\lambda^2-p^2}{k^2-p^2}\right]t_l(p,k;k^2)+\left[\frac{\lambda^2-k^2}{p^2-k^2}\right]t_l(k,p;p^2)$$
$$+\frac{4\mu}{\pi}(k^2-\lambda^2)(p^2-\lambda^2)\int_0^\infty dq\,q^2\frac{t_l(p,q;q^2)t_l^*(k,q;q^2)}{(\lambda^2-q^2)(p^2-q^2+i\epsilon)(k^2-q^2+i\epsilon)}\ . \tag{55}$$

This equation relates the fully-off-shell matrix elements to the half-shell matrix elements with arguments in the same region. The additional suppression factor in the demominator in the integral suggests that if p, k, and λ are all in the potential regime the information required to construct the matrix element $t_l(p,k;\lambda^2)$ is limited to the relative nucleon-nucleon wave functions for energies in the potential regime. This would explain the lack of model dependence of our results since our two models yield very similar wave functions in the potential regime, but differ significantly at energies and momenta above that.

D. Implications

Relation (55), together with the half-shell analyses of Picker, Redish, and Stephenson,[6] suggest that the near model independence of the fully-off-shell T matrix elements in the potential regime follows from the strongly constrained physical information common to most realistic potential models.

Our results suggest that the model dependence in nonrelativistic many-body calculations may be better understood if the calculations are formulated such that the T matrix is the two-body input. A sensitivity analysis of the output with respect to input T matrix elements should then be performed. If many-body results can be found which are sensitive only to the matrix elements in the potential regime, then we can expect the nonrelativistic results to have limited model dependence. Sharp tests of the model's validity may then be possible.

There are a number of possible examples which such a sensitivity analysis could be performed directly in existing calculations or in ones which are being currently developed.

In the three-nucleon bound-state problem such sensitivities were studied in the early 1970s. Levinger's[35] group at RPI and Lavine, Mukhopadhyay, and Stephenson[36] at Maryland both found that the three-body nucleon state for simple potentials (without short range repulsion) only required momenta up to about 2 fm^{-1}. More sophisticated calculations indicate that the use of more realistic potentials leads to sensitivities to somewhat larger momenta.[37]

The three-nucleon scattering problem seems to be dominated at low energies ($E_{\rm lab}\lesssim 50$ MeV) by the bound state and anti-bound-state poles in the ^3S-^3D and ^1S states, respectively,[38] though input from the P and D states is important in correctly predicting the spin observables.[39] Separable fits to realistic potentials do quite well here and may provide a clean case of a many-particle calculation with sensitivity limited to the potential regime.

A second case which needs to be analyzed from this point of view is the elastic and inelastic scattering of nucleons from nuclei in the low-intermediate energy region ($50\leq E_{\rm p}$ 350 MeV). Calculations based on the single-scattering approximation for the optical potential[40] and on the distorted-wave impulse approximation (DWIA) for inelastic transitions[41] do quite respectably in predicting some observables. There is also some indication that the calculations are not very sensitive to amplitudes far from the on-shell point.[42]

Unfortunately, all calculations either start from phenomenological amplitudes or employ a local-density approximation for the treatment of Pauli effects. Although the off-shell behavior of the phenomenological amplitudes are qualitatively similar to the off-shell amplitudes produced by potential models, they have not been studied sufficiently to determine whether they represent plausible models of the short range behavior of the nucleon-nucleon wave function. Those calculations that use realistic potential models do so by using a density dependent nuclear matter calculation and a local-density approximation whose validity is not well understood.[43] Both approaches will have to be developed with more care before one can conclude that this is an appropriate place to develop a sharp test of the nonrelativistic theory.[44]

The theory of nuclear matter is a third system in which it is natural to formulate the calculation in terms of the off-shell T matrix as two-body input by use of the reference spectrum method.[3,45] This approach gives the Brueckner G matrix as the solution of an equation for which the off-shell T matrix is the input. Unfortunately, most nuclear matter calculations take the Bethe-Goldstone equation as their starting point. This approach relies heavily on the coordinate space representation of the potential and thus mixes information in the potential regime with information from higher energies.

The wide variation of results obtained in nuclear matter with various realistic potentials[3] suggests that this is a case in which the potential regime is inadequate. Nevertheless, an analysis in terms of off-shell amplitudes could be quite instructive in helping us to understand what aspects of a nuclear matter calculation can plausibly be expected to be reliable in a nonrelativistic nucleons-only model. (Note that all potentials used in these calculations are not on-shell equivalent. Some of the sensitivity of the nuclear matter results may be a consequence of on-shell differences or of the inadequacies of particular approximations to the many-body calculation.)

We suggest that any many-particle calculation which requires information outside of the potential regime is not consistent even in principle with the philosophy of a nonrelativistic nucleons-only model. For such systems, at least the effects of deltas and mesons must be examined (and possibly other effects as well—see below). If no many-particle calculations exist which only require

information which is reasonably well determined by the procedure used to construct potentials, then the nonrelativistic framework would have to be declared a failure and not applicable to nuclear physics. (Even if this turns out to be the case, it might still be possible to use it as a phenomenology with a limited amount of information, such as bound state properties, calculated in some other framework.)

Broad questions of this character have come under active consideration in the nuclear community during the past few years. In particular, much attention has been given to the question: What are the appropriate fundamental degrees of freedom which should be used to describe nuclei? New formalisms which have been considered include (1) relativistic Dirac nucleons with meson exchange leading to strong coupling to the lower components,[46] (2) field theoretic models of point nucleons with mesons treated classically but dynamically (QHD),[47] (3) relativistic nonlocal models having only two spin components,[48] and (4) quark models with partial deconfinement.[49] These different approaches all give a picture of nuclei which is substantially different from traditional nonrelativistic nucleons-only model, and from each other.[44]

Each of these new formalisms produces improvement in some circumstances over the traditional model's predictions. In order for us to understand precisely what these successes imply, it would be exceedingly useful to analyze the results of these formalisms in terms of the effective pair and multiparticle interactions they lead to when they are forced into a nonrelativistic nucleons-only framework. If they only lead to modifications of the effective amplitudes outside the potential regime, then they are consistent with the nonrelativistic framework (which is necessarily limited in its range of applicability) and could be considered as a natural extension.

VII. CONCLUSIONS

In this paper we have compared the fully-off-shell behavior of the partial-wave T matrices produced by two very different realistic nucleon-nucleon potentials, the RSC and P80 potentials. The off-shell amplitudes are straightforward to calculate, and do not require large matrix inversions if the K-matrix equation is solved using the Sloan prescription for treating the principal value singularity. We also note that the convergence of the calculation for the phase shift (on-shell point) does not necessarily indicate convergence for the off-shell amplitudes. They must be tested separately.

Our main conclusions are the following:

(i) Although the two potentials look totally different in momentum space and have very different character (nonlocality), they yield off-shell amplitudes in the potential regime ($50 \leq E_{\rm lab} \leq 350$ MeV, k and $k' \lesssim 2$ fm^{-1}) which agree to within 20% in all states except the $^1P_1$ and better than that (5–10%) for the largest amplitudes.

(ii) Small disagreements (10–20%) in the fits to the phase shifts do not imply substantial disagreements of the off-shell amplitudes, though qualitative deviations in the energy dependence may signal qualitative differences off shell.

These points suggest that using the off-shell T matrix instead of the potential as two-body input to a many-body calculation may be a good way to focus on the model-dependent versus the model-independent features of the calculation. We have suggested a number of places where this might be profitably carried out.

ACKNOWLEDGMENTS

One of us (E.F.R.) is pleased to acknowledge the hospitality and support of the Indiana University Cyclotron Facility and Nuclear Theory Center, and the Los Alamos National Laboratory. Critical comments and suggestions by Alan Picklesimer are gratefully acknowledged. This work was supported in parts by Grants DE-FG05-87ER-40322, DE-AC02-81ER40047, and NSF-PHY86-06364.

*Permanent address: Department of Physics and Astronomy, University of Maryland, College Park, MD 20742.

[1]W. M. Kloet and J. A. Tjon, Ann. Phys. (N.Y.) **79**, 407 (1973); C. Stolk and J. A. Tjon, Nucl. Phys. **A295**, 384 (1978).

[2]A. K. Kerman, H. McManus, and R. M. Thaler, Ann. Phys. (N.Y.) **8**, 551 (1959); E. Siciliano and R. M. Thaler, Phys. Rev. C **16**, 1322 (1977); A. Picklesimer, P. C. Tandy, and R. M. Thaler, *ibid.* **25**, 1215 (1982).

[3]B. D. Day, in *From Nuclei to Particles,* "Enrico Fermi" School of Physics, Course 79, edited by A. Molinari (North-Holland, Amsterdam, 1981), p. 1.

[4]R. L. Workman and H. W. Fearing, Phys. Rev. C **34**, 780 (1986).

[5]E. F. Redish, G. J. Stephenson Jr., and G. M. Lerner, Phys. Rev. C **2**, 1665 (1970); E. F. Redish, G. J. Stephenson Jr., G. M. Lerner, and M. I. Haftel, *ibid.* **6**, 1559 (1972).

[6]H. S. Picker, E. F. Redish, and G. J. Stephenson Jr., Phys. Rev. C **4**, 287 (1971); E. F. Redish, G. J. Stephenson Jr., and H. S. Picker, *ibid.* **5**, 707 (1972); M. K. Srivastava and D. W. L. Sprung, Adv. Nucl. Phys. **8**, 121 (1975).

[7]R. V. Reid, Ann. Phys. (N.Y.) **50**, 411 (1968).

[8]M. Lacombe *et al.*, Phys. Rev. C **21**, 861 (1980).

[9]K. Erklenz, K. Holinde, and K. Bleuler, Nucl. Phys. **A139**, 308 (1969); R. Machleidt, K. Holinde, and C. Elster, Phys. Rep. **149**, 1 (1987).

[10]H. O. Klages, private communication; in *Proceedings of the International Workshop on Few-Body Approaches to Nuclear Reactions in Tandem and Cyclotron Energy Regions,* Tokyo, 1986, edited by S. Onyu and T. Sawado (World Science, Tokyo, 1987), p. 109.

[11]T. Sasakawa, Nucl. Phys. **A463**, 327c (1987); R. A. Brandenburg, Los Alamos National Laboratory Report LA-UR-86-3700, 1986.

[12]J. R. Taylor, *Scattering Theory* (Wiley, New York, 1972).

[13]B. A. Lippmann and J. Schwinger, Phys. Rev. **79**, 469 (1950).

[14]J. M. Blatt and L. C. Biedenharn, Phys. Rev. **86**, 399 (1952).

[15]H. P. Stapp, T. J. Ypsilantis, and N. Metropolis, Phys. Rev. **105**, 302 (1957).

[16]M. I. Haftel, F. Tabakin, Nucl. Phys. **A158**, 1 (1970).

[17]M. Abramowitz and I. A. Stegun, *Handbook of Mathematical*

Functions (National Bureau of Standards, Washington, D.C., 1964).

[18]B. D. Day, Phys. Rev. C **24**, 1203 (1981).

[19]W. N. Cottingham and R. Vinh Mau, Phys. Rev. **130**, 735 (1963); W. N. Cottingham *et al.*, *ibid.* D **8**, 800 (1973); R. Vinh Mau *et al.*, Phys. Lett. **44B**, 1 (1973); M. Lacombe *et al.*, Phys. Rev. D **12**, 1495 (1975); R. Vinh Mau, in *Mesons and Nuclei, Vol. I,* edited by M. Rho and D. Wilkinson (North-Holland, Amsterdam, 1979), p. 153.

[20]We are indebted to Professor S. Moszkowski for this observation.

[21]T. Hamada and I. D. Johnson, Nucl. Phys. **34**, 382 (1962); C. N. Bressel, A. K. Kerman, and B. Rouben, *ibid.* **A124**, 624 (1969); R. V. Reid, Ref. 7.

[22]F. Calogero and Yu. A. Simonov, Phys. Rev. Lett. **25**, 881 (1970).

[23]D. M. Brink and G. R. Satchler, *Angular Momentum* (Clarendon, Oxford, 1968).

[24]V. G. Neudatchin, Yu. F. Smirnov, and R. Tamagaki, Prog. Theor. Phys. **58**, 1072 (1977); A. Faessler, F. Fernandez, G. Luebeck, and K. Shimizu, Nucl. Phys. **A402**, 555 (1983); V. I. Kukulin, V. N. Pomerantsev, V. M. Krasnopol'sky, and P. B. Sazonov, Phys. Lett. **135B**, 20 (1984).

[25]I. H. Sloan, J. Comput. Phys. **3**, 332 (1968).

[26]K. L. Kowalski, Phys. Rev. Lett. **15**, 798 (1965); **15**, 908(E) (1965); H. P. Noyes, *ibid.* **15**, 538 (1965).

[27]M. Baranger, B. Giraud, S. K. Mukhopadhyay, and P. U. Sauer, Nucl. Phys. **A138**, 1 (1969).

[28]M. I. Haftel, Phys. Rev. Lett. **25**, 120 (1970).

[29]J. Friar, private communication.

[30]R. A. Ardnt, VPI and SU SAID Solution SM 86, private communication.

[31]W. Van Oers, in *International Symposium on the Three-Body Force in the Three-Nucleon System,* George Washington University, Washington, D.C., 1986, Vol. 260 of *Lecture Notes in Physics,* edited by B. Berman and B. Gibson (Springer, Vienna, 1987), p. 28.

[32]P. U. Sauer, in Ref. 31, p. 107.

[33]T. Fulton and P. Schwed, Phys. Rev. **115**, 973 (1959).

[34]R. F. Bishop, Phys. Rev. C **7**, 479 (1973).

[35]J. S. Levinger, in *Nuclear Physics,* Vol. 71 of *Springer Tracts in Modern Physics,* edited by G. Höhler (Springer, Berlin, 1974), p. 88.

[36]J. P. Levine, S. K. Mukhopadhyay, and G. J. Stephenson Jr., Phys. Rev. C **7**, 968 (1973).

[37]R. A. Brandenburg, Y. E. Kim, and A. Tubis, Phys. Rev. C **12**, 1368 (1975).

[38]R. Aaron, R. D. Amado, and Y. Y. Tam, Phys. Rev. **140**, B1291 (1965); R. T. Cahill and I. H. Sloan, Nucl. Phys. **A165**, 161 (1971).

[39]P. Doleschall, Nucl. Phys. **A201**, 264 (1973); **A220**, 491 (1974).

[40]G. W. Hoffmann, in Proceedings of the LAMPF Workshop on Dirac Approaches to Nuclear Physics, edited by J. R. Shepard, C. Y. Cheung, and R. L. Boudrie, Los Alamos Technical Report LA-10438-C, 1985, p. 28.

[41]C. Olmer, in *The Interaction Between Medium Energy Nucleons on Nuclei—1982,* AIP Cont. Proc. No. 97, edited by H. O. Meyer (AIP, New York, 1983), p. 176.

[42]A. Pickelsimer, P. C. Tandy. R. M. Thaler, and D. H. Wolfe, Phys. Rev. C **29**, 1582 (1984).

[43]L. Rikus and H. V. von Geramb, Nucl. Phys. **A426**, 496 (1984).

[44]E. F. Redish, in *Antinucleon and Nucleon-Nucleus Interactions,* edited by G. E. Walker, C. D. Goodman, and C. Olmer (Plenum, New York, 1985), p. 213.

[45]H. A. Bethe, B. H. Brandow, and A. G. Petchek, Phys. Rev. **129**, 225 (1963).

[46]S. J. Wallace, in Ref. 40, p. 87.

[47]B. Serot and J. D. Walecka, Adv. Nucl. Phys. **16**, 1 (1986).

[48]F. Coester and W. N. Polyzou, Phys. Rev. D **26**, 1348 (1982); B. Keister and W. N. Polyzou (unpublished).

[49]*Quarks and Nuclear Forces,* Vol. 100 of *Springer Tracts in Modern Physics,* edited by D. Fries and B. Seitnitz (Springer, Berlin, 1982).